Immunocapture of dsRNA-bound proteins provides insight into Tobacco rattle virus replication complexes

Marco Incarbone[1#], Baptiste Monsion[1], Lauriane Kuhn[2], Helene Scheer[1], Vianney Poignavent[1], Patrice Dunoyer[1] and Christophe Ritzenthaler[1*]

1. Institut de biologie de moléculaire des plantes, CNRS, Université de Strasbourg, France.

2. Plateforme protéomique Strasbourg Esplanade FR1589 du CNRS, Université de Strasbourg, Strasbourg, France.

Current address: Gregor Mendel Institute of Molecular Plant Biology (GMI), Vienna, Austria.

*Corresponding author

E-mail: ritzenth@unistra.fr (CR)

ABSTRACT

Plant RNA viruses form highly organized membrane-bound virus replication complexes (VRCs) to replicate their genome and multiply. VRCs contain both virus- and host-encoded proteins, and have been investigated through a number of experimental approaches, including genetic screens on surrogate model experimental hosts and pull-down of viral replicase proteins. Double-stranded RNA (dsRNA) is an obligate intermediate of the replication process of all RNA viruses and is the trigger of potent antiviral defenses in all eukaryotes. In this work, we describe the use of a GFP-tagged dsRNA-binding protein (B2:GFP) to pull down viral replicating RNA and associated proteins *in planta*. Following infection of *A. thaliana* constitutively expressing B2:GFP with *tobacco rattle virus* (TRV), we were able through GFP immunoprecipitation to pull down dsRNA. Mass spectrometry analysis of the dsRNA-B2:GFP-bound proteins from TRV-infected plants revealed the presence of (i) viral proteins such as the replicase, which attested to the successful isolation of VRCs, and (ii) a number of host proteins, some of which have previously been involved in virus infection. To verify whether the identified host proteins localized at TRV replication complexes, we selected nine candidates, generated genetic fusions with RFP, and transiently expressed them in healthy and TRV-infected *N. benthamiana* stably expressing B2:GFP. Confocal microscopy analysis revealed that eight out of nine candidates showed dramatic re-localization upon infection, and seven of these co-localized with B2-labeled TRV replication complexes, providing ample validation for the immunoprecipitation results. We therefore propose B2:GFP-mediated pull down of dsRNA to be a novel and robust method to explore the proteome of VRCs *in planta*.

AUTHOR SUMMARY

Viruses are an important class of pathogens that represent a major problem for human, animal and plant health. They hijack the molecular machinery of host cells to complete their replication cycle, a process frequently associated with the production of double-stranded RNA (dsRNA) that is regarded as a universal hallmark of infection by RNA viruses. Here we exploited the capacity of a GFP-tagged dsRNA-binding protein stably expressed in transgenic Arabidopsis to pull down dsRNA and associated proteins upon virus infection. In this manner we specifically captured short and long dsRNA from *tobacco rattle virus* (TRV) infected plants, and successfully isolated viral proteins such as the replicase, which attested to the successful isolation of virus replication complexes (VRCs). More excitingly, a number of host proteins, some of which have previously been involved in virus infection, were also captured. Remarkably, among a set of nine host candidates that were analyzed, eight showed dramatic re-localization to viral factories upon infection, and seven of these co-localized dsRNA-labeled VRCs. Being compatible with any plant virus as long as it infects Arabidopsis, we propose our dsRNA-centered strategy to be a novel and robust method to explore the proteome of VRCs *in planta*.

INTRODUCTION

Viruses are obligate endocellular parasites that hijack their host's molecular processes and machinery to multiply, a process that sometimes results in devastating diseases. Pivotal to a successful infection is the efficient replication of the viral genomic nucleic acid(s). In the majority of plant virus species the genome consists of one or more molecules of single-stranded positive polarity RNA, or (+)ssRNA. Replication is carried out by the virus-encoded RNA-dependent RNA-polymerase (RdRp), often part of a larger protein known as the replicase. This enzyme first copies the viral (+) genome into (-)ssRNA that is then used as a

76 template for the production of progeny (+)ssRNA. Intrinsic to the RNA replication process is
77 the generation of long double-stranded RNA (dsRNA) intermediates by the viral RdRp.
78 The replication of all known (+) strand RNA virus takes place on host membranes whose
79 origin, whether the endoplasmic reticulum, chloroplasts, mitochondria, peroxisomes etc…,
80 depends on virus species (reviewed in [1-4]). The progressive virus-induced recruitment of
81 such membranes generally leads to dramatic reorganizations of the host endomembrane
82 system into so called "viral factories". These viral factories are the sites where all steps vital
83 to the virus life are carried out including protein translation, RNA encapsidation and RNA
84 replication *sensu stricto*. The specialized molecular entities on which RNA replication occurs
85 within the viral factories are known as the virus replication complexes (VRCs). While a
86 minimal VRC arguably consists of single- and double-stranded viral RNA and replicase, their
87 precise composition, which depends on the virus and host species, remains largely
88 unexplored. A number of studies have shown that specific host proteins can be integral part
89 of these VRC and exert positive (pro-viral) or negative (anti-viral) effects on replication. Our
90 knowledge on these host proteins is summarized in several exhaustive reviews [5-7]. These
91 include among others RNA-binding proteins, RNA helicases, chaperones and proteins
92 belonging to the RNA interference machinery (RNAi, or RNA silencing), which is the
93 primary response to replicating viruses in plants and other eukaryotes [8, 9].
94 Antiviral RNAi against RNA viruses in model plant species *A. thaliana* is initiated by
95 RNAse-III Dicer-Like enzymes DCL4 and DCL2, which cleave dsRNA into 21- and 22-nt
96 small-interfering RNA (siRNA), respectively. These siRNA are then loaded into Argonaute
97 (AGO) proteins, which use them as templates to recognize and cleave viral ssRNA in a
98 sequence-specific manner. Viruses have evolved a vast array of strategies to evade or block
99 RNAi, the best studied of which are viral suppressors of RNA silencing (VSRs). These
100 proteins suppress silencing through a wide range of molecular strategies, from inhibition of

101 dicing, to siRNA sequestration, to AGO degradation [10]. Of note, *A. thaliana* encodes
102 several RNAse-III-like enzymes (RTLs) in addition to Dicers, but little is known regarding
103 their function [11, 12]. The accumulation of viral dsRNA *in planta* varies widely among
104 (+)ssRNA virus and host species, as we have recently shown [13]. While the precise
105 molecular events occurring during virus RNA replication are often unclear, it can be argued
106 that rapid and efficient separation of the (+) and (-) RNA strands could not only allow more
107 replication cycles to take place, but also constitute a powerful mechanism of RNA silencing
108 evasion/suppression through removal of dsRNA.
109 A great deal of our knowledge on plant virus VRCs emerged from a series of seminal studies
110 conducted with *Tomato bushy stunt virus* (TBSV) on yeast, a surrogate host used as a
111 powerful biological tool to conduct genetic screens and functional studies on host factors
112 involved in TBSV VRC activity (reviewed in [5]). While the authors of these studies, where
113 possible, validated the results obtained in yeast and *in vitro* on plant species *N. benthamiana*,
114 data obtained *in planta* on VRCs of other viruses remains sparse. Recent studies have
115 reported methods to spatio-temporally visualize VRCs *in vivo* via fluorescently labeled
116 dsRNA-binding proteins [8, 13, 14]. Candidate-based, reverse genetic approaches have been
117 used to probe the involvement of host factors in VRC formation and activity in plants [15,
118 16]. These approaches, however, are necessarily based on prior discovery acquired by other
119 experimental means. Another experimental strategy successfully used to characterize VRCs
120 has been to pull down tagged viral proteins and analyze the resulting protein populations by
121 mass spectrometry [17-19]. While this last method has provided valid and compelling data,
122 we decided to investigate VRCs from a viral RNA-centered, rather than viral protein-
123 centered, perspective. We hypothesized that pull-down of dsRNA from virus-infected plants
124 followed by mass spectrometry of dsRNA-associated proteins would provide insight into the
125 molecular composition of VRCs.

126 To test this hypothesis, we used the eGFP-tagged dsRNA-binding domain of FHV protein
127 B2, which we have previously used to efficiently detect viral dsRNA *in vitro* and in
128 constitutively-expressing *N. benthamiana* [13]. *Arabidopsis thaliana* being more appropriate
129 for genetic studies than *N. benthamiana*, we first generated transgenic *A. thaliana* Col-0
130 plants stably expressing B2:GFP. We infected them with *Tobacco rattle virus* (TRV), a well-
131 studied (+)ssRNA virus, performed GFP immunoprecipitation and identified
132 immunoprecipitated proteins by LC-MS/MS. In this manner, a number of virus- and host-
133 encoded proteins could be identified. To validate their localization at B2:GFP-labeled TRV
134 replication complexes, we tagged these candidates with tagRFP (tRFP hereafter) [20],
135 transiently expressed them in healthy vs. TRV-infected 35S:*B2:GFP*/*N. benthamiana* [13]
136 and observed the resulting leaf tissues by confocal laser scanning microscopy. We found that
137 eight out of the nine *A. thaliana* proteins tested, including factors that have never before been
138 linked to virus infection, re-localized strictly to B2:GFP-labeled TRV VRCs or alternatively
139 to the larger TRV-induced viral factories. These results provide robust validation of dsRNA
140 pull-down as an effective and high-throughput method for VRC characterization *in planta*.
141 Furthermore, the results offer detailed snapshots of TRV replication complexes and viral
142 factories, with host factors showing unique and distinct localization patterns in and around
143 these complexes.
144

145 **RESULTS**

146 **B2:GFP-mediated isolation of Tobacco rattle virus dsRNA from *A. thaliana***

147 The double-stranded RNA-binding B2:GFP protein, when ectopically expressed in transgenic
148 35S:*B2:GFP*/*N. benthamiana*, has been previously shown to specifically associate with the
149 VRCs of several positive-strand RNA viruses from plants and insects [13]. Following these
150 findings, we wished to further exploit B2:GFP as a biochemical bait to explore the

151 composition and biology of RNA VRCs, the pivotal element of which is dsRNA. To do so,
152 and given the versatility of *A. thaliana* as a model plant species, we first produced
153 homozygous 35S:*B2:GFP* transgenic plants. Although in this work we focused essentially on
154 the 35S:*B2:GFP/*Col-0 line, 35S:*B2:GFP* was also introduced into various genetic
155 backgrounds including mutants of the core antiviral Dicer-Like genes, *dcl2-1*, *dcl4-2* and
156 triple *dcl2-1/dcl3-1/dcl4-2* (**Supplementary Figure 1A,B,C**). The rationale behind this
157 choice is that DCL proteins are arguably the best-known RNAse III enzymes in plants, and
158 the small-interfering RNA (siRNA) they generate from virus-derived dsRNA precursors are
159 the effectors of RNA silencing, the main antiviral defense in plants [10, 21]. Similarly to the
160 B2:FP *N. benthamiana* lines [13] and despite the clear expression of B2:GFP
161 (**Supplementary Figure 1A),** the different lines showed little to moderate developmental
162 phenotypes (**Supplementary Figure 1C**). These were very reminiscent of - but distinct from
163 - those caused by ectopic expression of other RNA silencing suppressors such as P19 or HC-
164 Pro [22, 23]. Such phenotypes may be determined (i) by inhibition of long dsRNA processing
165 into siRNA or (ii) by disruption of miRNA function through their sequestration, or both.
166 The full-length FHV B2 protein has been shown to be a suppressor of RNA silencing [24,
167 25], and proposed to act through both inhibition of dicing and sequestration of siRNA [26].
168 To investigate whether the GFP-tagged 73 amino acid dsRNA binding domain of B2 that
169 lacks the residues involved in the interaction with PAZ domains of Dicer proteins [27, 28]
170 also acts as a suppressor of RNA silencing, we performed a standard GFP silencing patch test
171 on *N. benthamiana* leaves (**Supplementary Figure 1D,E**). B2, as a C-terminal fusion to
172 tRFP (B2:tRFP) was able to suppress silencing of the GFP transgene, as was *Turnip crinkle*
173 *virus* suppressor P38. By contrast, a C44S, K47A double-mutated version of B2:tRFP
174 impaired in dsRNA binding [13] was unable to suppress silencing, suggesting that
175 suppression activity is dsRNA-binding-dependent and likely DCL-binding-independent.

176 Next, we investigated the effects of stably expressed B2:GFP on endogenous small RNA
177 pathways: biogenesis of microRNAs 159 and 160 was not perturbed in 35S:*B2:GFP*/Col-0
178 plants, while biogenesis of siRNA such as endo-siRNA (IR71) and *trans*-acting siRNA
179 (TAS1) was completely abolished (**Supplementary Figure 1B**). Whether these defects in
180 endo-siRNA and *trans*-acting siRNA biogenesis are responsible of the observed
181 developmental phenotypes remains to be determined.
182 Once characterized molecularly, we infected 35S:*B2:GFP*/Col-0 plants with a recombinant
183 TRV carrying part of the phytoene desaturase (PDS) gene [29]. As expected, the control Col-
184 0 plants showed minor viral symptoms and the typical bleaching phenotype linked to PDS
185 gene silencing. In contrast, the B2:GFP-expressing plants showed no significant leaf
186 discoloration but severe viral symptoms (**Figure 1A**) and death of the plants occurred before
187 flowering (not shown), well in agreement with the efficient RNA silencing suppression
188 activity of the B2 dsRNA-binding domain. Observation of systemically infected leaves by
189 confocal microscopy showed TRV-induced re-localization of B2:GFP to distinct cytosolic
190 mesh-like structures (**Figure 1B**) very reminiscent to those observed in 35S:*B2:GFP*/*N.*
191 *benthamiana* and shown to correspond to TRV-induced VRCs [13]. Northern analysis of
192 RNA from TRV-PDS systemically infected 35S:*B2:GFP*/*N. benthamiana* and
193 35S:*B2:GFP*/Col-0 revealed that B2:GFP caused a striking over-accumulation of viral
194 (+)ssRNA in both plant species (**Figure 1C**). This is also in agreement with B2:GFP activity
195 as a suppressor of RNA silencing, and could be recapitulated in a *dcl2-1/dcl4-2* double
196 mutant (*dcl24*), which lacks the two main antiviral Dicers (**Supplementary Figure 1F**)[30].
197 In line with the over accumulation of viral (+)ssRNA, B2:GFP also caused a tremendous
198 increase in long double-stranded RNA content, likely corresponding to replication
199 intermediates, as determined by northwestern blotting in both B2:GFP-expressing Col-0 and
200 *N. benthamiana* plants (**Figure 1D**). In contrast, TRV-derived siRNA were differentially

201 regulated between Arabidopsis and *N. benthamiana*. Thus, while B2:GFP expression led to
202 an overall reduction in 21 and 22 nt vsiRNA species in Col-0 plants, the opposite effect was
203 observed in *N. benthamiana* (**Figure 1E**). Conversely, miR159 and U6-derived snRNA
204 accumulation was unaffected by the presence of B2:GFP in both plant species (**Figure 1E**,
205 **Supplementary Figure 1B**). These results suggest that B2:GFP interferes strongly with TRV
206 RNA processing by DCL enzymes, thereby promoting viral replication.
207 As a first experiment establishing B2:GFP as a tool to study VRCs, we performed anti-GFP
208 immunoprecipitations (IPs) from TRV-PDS-infected 35S:*B2:GFP*/Col-0 plants and analyzed
209 their composition in (+)strand viral RNA (**Figure 1C**), long dsRNA (**Figure 1D**), siRNA
210 (**Figure 1E**) and proteins (**Figure 1F**). As a negative control, we included TRV-PDS-infected
211 35S:*GFP*/Col-0 plants. Northern and northwestern analyses performed on IPed RNA
212 revealed that immune complexes contained (+)ssRNA, long dsRNA and 22nt vsiRNA, but no
213 U6 and miR159 (**Figure 1C-E**). Interestingly, and in contrast with our previous report *in*
214 *vitro* [13] but well in agreement with the capacity of B2 to bind dsRNAs longer than 18 bp
215 [26], antiviral siRNA were immunoprecipitated (**Figure 1E**). Western analysis of proteins
216 from the same experiment revealed efficient IP of both GFP and B2:GFP (**Figure 1F**).
217 Altogether we concluded that immunoprecipitation allowed the isolation of TRV double-
218 stranded replication intermediates, the core element of VRCs.
219

220 **Immunoprecipitation and identification of B2:GFP-associated viral and host proteins**
221 **by mass spectrometry**

222 Once established that immunoprecipitation of B2:GFP from plants allowed efficient isolation
223 of virus replication dsRNA intermediates, we wondered whether these complexes contain
224 specific virus- and host-encoded proteins. To address this question we performed anti-GFP IP
225 on TRV-PDS-infected 35S:*GFP*/Col-0 vs. 35S:*B2:GFP*/Col-0 in triplicate, and analyzed the

226 immunoprecipitated proteins by mass spectrometry (MS). A preliminary analysis by
227 immunoblot confirmed efficient and reproducible B2:GFP and GFP immunoprecipitation
228 (**Supplementary Figure 2**), which could be confirmed by MS, reads from B2:GFP and GFP
229 being the most abundant **(Figure 2A,B, Supplementary Table 2**). We next searched and
230 ranked accessions that were identified only - or highly enriched - in 35S:*B2:GFP*/Col-0
231 samples (**Figure 2A,B**, **Supplementary Table 2**). As expected, the TRV RNA-dependent
232 RNA-polymerase (Uniprot accession Q9J942) was among the most abundant proteins
233 detected in immunoprecipitates from B2:GFP samples and was absent from GFP samples
234 (**Figure 2**). This result, along with the previously described detection of viral dsRNA in
235 analogous IPs (**Figure 1**), suggests that B2:GFP immunoprecipitation allows the isolation of
236 *bona fide* TRV VRCs. This hypothesis is further supported by the detection of TRV coat
237 protein (CP, Uniprot Q88897) and 16k suppressor of silencing (Uniprot Q77JX3) in B2:GFP
238 immunoprecipitates (**Figure 2**). It also suggests that the 16k and CP associate directly or
239 indirectly to dsRNA. Although unlikely, we can't at this point rule out that one or more of
240 these TRV proteins bind B2:GFP and not dsRNA. In addition to TRV-encoded proteins, MS
241 analysis allowed also the identification of 110 host proteins exclusively present in
242 immunoprecipitates from B2:GFP-expressing plants (**Figure 2** and **Supplementary Table**
243 **2**), which we considered as replication complex-associated host protein candidates. Volcano
244 plot analysis revealed that out of these proteins, 29 presented an adjusted p-value < 0.05
245 (**Figure 2B)**.
246 With the aim to evaluate the association of candidate host proteins to replication complexes
247 and considering their high number, we first established a priority list of nine *A. thaliana* gene
248 products that were either detected with high spectral counts (AT5G02500, AT3G09440,
249 AT3G12580) or confirmed/potential RNA-binding/interacting proteins from literature or
250 NCBI annotation (AT1G24450, AT5G04430 [31], AT3G62800 and AT2G28380 [32]), or

251 both (AT1G23410, AT3G45570)(**Figure 2A,B**). We excluded from our priority list a number
252 of proteins that were significantly enriched in infected vs. non-infected plants due to the
253 number of candidates to analyze and their apparent lack of significance in viral replication
254 process based on literature. This includes for instance the most enriched protein, a
255 myrosinase present in Brassica crops with anti-microbial activity and involved in defense
256 against herbivores [33].
257
258 **tRFP does not label TRV replication complexes *in planta***
259 In a second step, we tested the subcellular localization of the selected candidates in relation to
260 B2:GFP in healthy and TRV-infected plants. To do so, we opted for the 35S-driven transient
261 expression of the Arabidopsis candidates as N- or C-terminal fusions to tRFP in healthy or
262 TRV-infected 35S:*B2:GFP*/*N. benthamiana*, as described in the methods section. In all cases,
263 confocal imaging was performed 3-4 days post agro-infiltration, a time that was found to be
264 optimal for TRV-infection and transient expression of protein candidates.
265 As an absolute prerequisite to our validation pipeline of candidate proteins and considering
266 tRFP was used as reporter tag, we first carefully analyzed the intracellular distribution of
267 tRFP with respect to TRV replication complexes in 35S:*B2:GFP*/*N. benthamiana*. As
268 expected, tRFP as well as B2:GFP showed a typical nucleo-cytoplasmic localization in cells
269 from healthy plants (**Figure 3A**), well in agreement with our previous report using the same
270 experimental system [13]. Crucially, upon infection the intracellular distribution of tRFP
271 remained unchanged, while B2:GFP concentrated to bright cytoplasmic cotton-ball-like
272 structures often adjacent to the nucleus (**Figure 3B**). These large structures were previously
273 shown to correspond to TRV viral factories enriched in mitochondria-derived membranes
274 [13] on which replication of TRV is thought to occur [34]. Importantly, our data clearly show
275 that while B2:GFP is highly enriched in TRV replication factories, tRFP alone is significantly

276 depleted from these structures (**Figure 3B**), in agreement with the behavior of tRFP as
277 cytoplasmic and validating tRFP as a reporter protein with which to tag the candidates of
278 interest.
279
280 **Double-stranded RNA-binding proteins (DRBs) perfectly colocalize with B2-labeled**
281 **viral replication complexes**
282 DRBs are proteins with dual dsRNA-binding motifs with five representatives in the
283 Arabidopsis genome [32, 35]. Despite showing low spectral counts in our IPs, two DRBs
284 were identified in our analysis: DRB2 (AT2G28380, total counts: 4, **Figure 4A**) and DRB4
285 (AT3G62800, total counts: 5, **Figure 4A**) that were obvious candidates to test (**Figure 4**).
286 DRB2 was recently shown to localize to the replication complexes of different RNA viruses
287 [8], to be able to bind dsRNA [36] and to play a role in endogenous small RNA biogenesis
288 [32, 37, 38]. In non-infected plants DRB2:tRFP and B2:GFP localized to rather distinct
289 cytoplasmic and nuclear structures, whereas a near-perfect colocalization of DRB2:tRFP and
290 B2:GFP was observed in the VRCs upon TRV-PDS infection (**Figure 4B**), which was
291 particularly evident at high magnification (**Figure 4C)**. Remarkably, while DRB2:tRFP was
292 almost exclusively found in the cytoplasmic VRCs upon infection, a substantial fraction of
293 B2:GFP remained associated to nuclear structures likely containing dsRNA (**Figure 4C**).
294 This suggests that although both proteins are susceptible to bind dsRNA, their intracellular
295 targeting is likely not exclusively dsRNA-dependent.
296 DRB4 has been shown to be both a co-factor of DCL4 in small RNA biogenesis and an
297 inhibitor of DCL3 in endogenous inverted-repeat RNA processing in *A. thaliana* [39, 40].
298 More relevantly here, DRB4 is involved in the defense against RNA viruses [41, 42]. When
299 we expressed DRB4:tRFP in non-infected tissue, this protein accumulated predominantly to
300 the nucleus where it colocalized with B2:GFP (**Figure 4D**), in agreement with previous

301 reports [8, 13]. Upon TRV infection DRB4:tRFP was clearly redistributed to VRCs, where it
302 perfectly colocalized with B2:GFP (**Figure 4D, E**). In contrast with DRB2, that was barely
303 detectable in the nucleus, a significant fraction of DRB4:tRFP remained nuclear upon
304 infection (**Figure 3D, E**).
305 Altogether, the robust colocalization of both double-stranded RNA-binding proteins DRB2
306 and DRB4 with B2:GFP during infection provide (i) further evidence that the TRV-viral
307 factories are indeed cytoplasmic dsRNA hotspots and, more importantly, (ii) a first validation
308 of the immunoprecipitation procedure.
309
310 **Proteins previously linked to viral infection localize at/near VRCs**
311 A family of proteins that emerged with high spectral counts were those belonging to the
312 HSP70 family: HSP70 (AT3G12580, 63 counts), HSP70-1 (or HSC70-1, AT5G02500, 81
313 counts) and HSP70-3 (or HSC70-3, AT3G09440, 71 counts) (**Figure 5A**). Members of this
314 family of chaperones have been shown in several studies to play key roles in virus infection
315 cycles (reviewed in [5, 43]). They can regulate viral life cycles both positively and
316 negatively, and depending on the virus, they affect VRC formation, virus movement and coat
317 protein homeostasis, among other processes. Three recent studies showed that unrelated plant
318 viruses hijack HSP70 to greatly enhance virus replication [44-46].
319 All three HSP70 members were tested in TRV-infected **(Figure 5)** and non-infected
320 **(Supplementary Figure 3)** 35S:*B2:GFP*/*N. benthamiana*. When overexpressed in healthy
321 plants HSP70:tRFP, HSP70-1:tRFP, HSP70-3:tRFP localized essentially to distinct
322 cytoplasmic foci whose number, size and distribution were specific for each of the three
323 HSP70 observed (**Supplementary Figure 3**). Remarkably, upon infection, HSP70-1:tRFP
324 **(Figure 5C)** and HSP70-3:tRFP **(Figure 5D)** were clearly redistributed to TRV viral
325 factories enriched in B2:GFP. In contrast, the localization pattern of HSP70:tRFP remained

326 essentially unaffected upon infection, with no obvious colocalization of B2:GFP with
327 HSP70:tRFP-labeled foci **(Figure 5B, Supplementary Figure 3A)**.
328 It should be noted that despite the clear redistribution of HSP70-1:tRFP **(Figure 5C)** and
329 HSP70-3:tRFP upon infection, only partial colocalization was detected between these
330 proteins and B2:GFP **(Figure 5C,D)**. The latter appeared engulfed in large HSP70-1 or
331 HSP70-3-containing bodies, likely corresponding to larger viral factories. This sub-
332 localization is in sharp contrast with the near perfect colocalization of B2:GFP with DRB2
333 and DRB4 upon infection (**Figure 4**). Altogether our results suggest that HSP70-1 and
334 HSP70-3, contrarily to HSP70, are *bona fide* components of the TRV viral factories.
335 However, contrarily to B2, DRB2 and DRB4 that directly interact with dsRNA, HSP70-1 and
336 HSP70-3 are likely involved in indirect interactions with TRV replication complexes,
337 perhaps via the TRV replicase or other viral or host components. Interestingly, it has recently
338 been observed using the B2:GFP system that dsRNA-containing VRCs constitute only a part
339 of the structures induced by PVX, which in fact also contain viral ssRNA and coat protein
340 [13]. The components and activities harbored within these larger "viral factories" are still
341 largely unknown, but the localization patterns of HSP70-1 and HSP70-3 suggests that these
342 proteins associate not only to replication complexes but also to other entities within viral
343 factories.
344 Next, we tested the localization of an RNA-binding protein present in our IP MS list that was
345 previously shown to associate to plant virus RNA. This protein, known as Binding to ToMV
346 RNA (BTR1, AT5G04430, 7 counts), was identified through affinity purification of tagged
347 viral RNA and found *in vitro* to bind to the 5' region of the (+) polarity RNA of ToMV, a
348 tobamovirus [31]. In our experimental system, BTR1:tRFP localized to numerous
349 cytoplasmic punctate structures at the cell periphery in non-infected cells **(Supplementary**
350 **figure 3D)**. Upon TRV-PDS infection, BTR1 was seen to clearly localize at B2:GFP-labeled

351 VRCs, while to some extent maintaining the localization visible in non-infected cells. At high
352 magnification it is possible to see that BTR1 did not strictly and exclusively colocalize with
353 B2:GFP, but could also be seen in the areas surrounding B2:GFP-labeled dsRNA hotspots
354 (**Figure 5E**). Similarly to HSP70-1 and HSP70-3, it is possible that BTR1 associates not only
355 to VRCs but also to other entities within viral factories.
356
357 **Novel proteins are localized at/near replication complexes**
358 Among the potential TRV replication complex-associated proteins identified through IP, we
359 tested three on which we found no specific function in virus process from the literature: a
360 RING/U-box protein (AT3G45570) and Ribosomal Protein S27a (AT1G23410), both
361 detected with relatively high spectral counts, and NFD2 (Nuclear Fusion Defective 2 –
362 AT1G24450)(**Figure 6A**).
363 The RING/U-box protein, which we will refer to as RUP1, belongs to the E3 ubiquitin ligase
364 RBR family. The N-terminal half of the protein is homologous to the RNAse H superfamily,
365 followed on the C-terminal half by a RING-type zinc-finger domain and an IBR (In Between
366 Ring fingers) domain. The Ribosomal Protein 27a, here abbreviated to RP27a, is a small
367 protein of 156 aminoacids with a ubiquitin domain N-terminal half and a zinc-binding
368 ribosomal protein superfamily C-terminal section. Importantly, all RP27a peptides detected
369 in B2:GFP co-immunoprecipitated samples belong to the ubiquitin domain, and also match
370 with the protein sequences of UBQ1 through UBQ14 (**Supplementary Figure 5**). This
371 suggests ubiquitination of one or more proteins present in the immunoprecipitates that
372 possibly associated to TRV replication complexes. To investigate which protein/s were
373 ubiquitinated, we searched the mass spectrometry dataset for di-glycine footprints, a hallmark
374 of ubiquitination. Interestingly, the only protein found to contain such a feature was RP27a
375 itself, only on lysine-48 (**Supplementary Figure 5**), suggesting self-ubiquitination and/or the

376 formation of lysine-48 polyubiquitin chains. Given that no other di-glycine footprint was
377 found in our spectrometry dataset, the proteins targeted by these chains may have been below
378 detection level and remain to be identified. Finally, NFD2 was first identified as a factor
379 involved in karyogamy, the fusion of polar nuclei within the central cell of the female
380 gametophyte prior to fecundation and the fusion of the sperm cells' nuclei with the egg cell
381 and the central cell upon fecundation [47]. This protein, containing an RNAse III domain, has
382 been also described as RNAse Three-Like 4 (RTL4) [11].
383 In healthy cells, tRFP-tagged RUP1 and RP27a displayed a nucleo-cytoplamic distribution
384 (**Supplementary Figure 4A,B)**, while NFD2 was essentially found in numerous cytoplasmic
385 bodies (**Supplementary Figure 4C)**. Upon TRV infection, all three proteins were clearly re-
386 localized to or near B2:GFP-labeled dsRNA hotspots (**Figure 6**, **Supplementary Figure 4).**
387 More precisely, RUP1 and RP27a showed patterns similar to those observed with HSP70-1,
388 with extensive overlap with B2:GFP as seen from the white color in the merged panels
389 (**Figure 6B,C)**. This suggests that RUP1 and RP27a associate not only with VRCs but also to
390 other entities within viral factories. Interestingly, NFD2 showed a pattern of localization
391 different from the other proteins tested in this work (**Figure 6D, Supplementary Figure 4C)**.
392 Although localization of NFD2 and B2 seemed mutually exclusive, NFD2 being absent from
393 B2:GFP-labeled structures and vice versa, a continuum between B2:GFP-labeled hotspots
394 and NFD2-labeled structures was observed (**Figure 6D**), suggesting that NFD2 is intimately
395 linked to TRV-induced subcellular entities and was therefore immunoprecipitated. In
396 addition, the complete localization of NFD2 in close proximity to TRV replication complexes
397 was in stark contrast with the perinuclear and cytoplasmic point-form localization of NFD2 in
398 non-infected plants **(Supplementary Figure 4C**).
399
400 **DISCUSSION**

401

402 We have here provided a description of a novel approach toward the identification of VRC-
403 associated proteins through the isolation of replicating viral dsRNA during genuine infection,
404 and validated the localization of most of the candidates through a rapid, robust and simple
405 system. Although the proof of concept is established here only for TRV, this approach should
406 be compatible with any plant virus as long as it is able to produce dsRNA during its
407 replication cycle. Importantly, it does not involve as a prerequisite any modification of viral
408 genomes, the production of infectious clones or the specific tagging of viral protein. Also,
409 considering the isolation of viral dsRNA and associated proteins is achieved indirectly by
410 anti-GFP antibodies, there is no requirement for virus- or dsRNA-specific antibodies in the
411 process. Hopefully this experimental approach will provide future investigators with a
412 universal tool to successfully explore the proteome associated to the replication complexes of
413 their favorite RNA virus, which can then be studied more in detail to discover the function of
414 VRC-associated proteins and their involvement in the viral life cycle. As hosts,
415 35S:*B2:GFP*/*A. thaliana* (this study) and 35S:*B2:GFP*/*N. benthamiana* [13] are compatible
416 with numerous plant virus species. If needed, the systems could be easily adapted to other
417 plant species, as long as they accommodate stable transformation.
418 We have shown that ectopic expression of B2:GFP greatly increases the accumulation of
419 TRV RNA both in *A. thaliana* and *N. benthamiana*. Given the activity of the 73 amino-acid
420 double-stranded binding domain of B2 as a VSR (this work), it is tempting to ascribe TRV
421 over-accumulation simply as a consequence of RNA silencing suppression and subsequent
422 enhanced viral replication. While this is very probably the case, it cannot be excluded that
423 B2:GFP increases TRV accumulation by other means independent of RNAi, such as
424 stabilization of dsRNA or its protection from other host defensive pathways. Preliminary data

425 also suggest that enhanced viral replication may not be restricted to TRV but likely applies to
426 other RNA virus (Ritzenthaler, unpublished)
427 The drastic effect of B2:GFP on TRV infection can be viewed as a double-edged sword in
428 relation to its use as bait to pull down VRCs. On one hand, this effect may introduce biases of
429 both quantitative and qualitative nature, such as the unspecific association to VRCs of host
430 proteins that do not play a role during infection in wild-type conditions or changes in the
431 accessibility or protein complement of replicating RNA, for example. On the other hand, the
432 over-accumulation of TRV dsRNA constitutes a real advantage for the study of VRCs. In
433 fact, increased viral replication is in favor of (i) a better immunoprecipitation efficiency, (ii)
434 an enhanced detection of protein partners by mass spectrometry and (iii) an improved
435 visualization of VRCs with test candidates. While these biases clearly need to be taken into
436 account, we strongly believe that overall this approach has far more advantages than
437 drawbacks.
438 The abundance of TRV replicase detected in the IPs is, in our opinion, confirmation of the
439 robustness of the experiment in terms of VRC yield and integrity. The abundant detection of
440 the coat protein suggests that it either plays a direct role in TRV replication or that the VRCs
441 present in the IPs contain not only full-length dsRNA, but also (+)ssRNA that is being
442 encapsidated, possibly during or just after separation from the (-) strand. However, despite
443 the use of detergent during the IPs, it is possible that we have pulled down proteins present
444 on membranes or complexes close to the replication organelles but not actually part of them.
445 Remarkably, among the nine candidate *A. thaliana* proteins detected following B2 IP and
446 tested in this work, only one, HSP70, failed to accumulate in VRCs despite a high spectral
447 count. HSP70 has been linked to viral infection in a number of papers [5, 43] and found to
448 directly bind the viral replicase in at least two studies [48, 49]. It is possible that the tRFP
449 could have disrupted the function of the protein. Another possibility is that the *A. thaliana*

450 HSP70 (AT3G12580) may not be fully functional when expressed in the heterologous host *N.*
451 *benthamiana.*
452 All remaining 8 candidates were specifically redistributed upon infection, suggesting
453 involvement of these factors in the viral life cycle. Their localization patterns can be divided
454 into three groups: perfect co-localization (DRB2 and DRB4), partial co-localization (HSP70-
455 1, HSP70-3, BTR1, RUP1 and RP27a) and proximity (NFD2).
456 Perfect co-localization most likely reflects the direct association of DRB2 and DRB4 on
457 replicating dsRNA within the VRCs. This result is in line with the experimentally verified
458 ability of DRB2 and DRB4 to bind dsRNA [36, 50] and of DRB4 to bind TYMV dsRNA *in*
459 *vivo* [41]. DRB2 was recently shown in *A. thaliana* to re-localize to cytoplasmic punctate
460 bodies upon infection by TuMV, TSWV and TYMV [8] and DRB4 to re-localize from nuclei
461 to cytoplasmic VRCs upon TYMV infection [41]. While DRB4 plays a role in antiviral
462 defense [41, 42] as part of the RNA silencing machinery, the function of DRB2 recruitment
463 to replication complexes, if any, remains to be uncovered. Although additional experiments
464 are required to confirm the direct association of DRB2 and DRB4 to TRV replicating
465 dsRNA, our data suggest that host proteins including antiviral defense protein such as DRBs
466 may have access to vdsRNA within replication organelles. This potentially questions the
467 suggested function of replication organelles as protective structures against degradation by
468 cellular RNases and detection by putative dsRNA sensors that trigger antiviral responses [51-
469 53].
470 The pattern of partial co-localization, observed for HSP70-1, HSP70-3, BTR1, RUP1 and
471 RP27a/Ubiquitin, consisted in the localization at the B2-labeled VRCs *per se*, as well as
472 features in close proximity, generally designated as "viral factories". In the case of PVX, the
473 dsRNA-containing replication complexes reside within larger viral factories harboring other
474 viral proteins and viral ssRNA [13]. In general, these viral factories are most likely the hub

475 for a plethora of viral activities beyond RNA replication *sensu stricto,* such as translation,
476 encapsidation, etc…, and which likely require specific host-encoded proteins. Our work
477 suggests that HSP70-1, HSP70-3, BTR1, RUP1 and RP27a/Ubiquitin may play such
478 functions during replication of TRV and possibly other viruses. Indeed, HSP70-3 and BTR1
479 have been shown to interact with TuMV replicase [17] and ToMV ssRNA [31], respectively.
480 Similarly, ubiquitin and the ubiquitin pathway have been shown in a number of studies to
481 play important roles in plant virus life cycle, both pro-viral and anti-viral, the details of which
482 are exhaustively reviewed in [54, 55]. Finally concerning NFD2, the pattern of proximity
483 suggests that this protein may indirectly be involved in viral factory function without directed
484 association with viral dsRNA per se. A proper validation of all these candidates by genetic
485 and cell biology approaches is now required, but is outside the scope of this manuscript and
486 will be addressed in further studies.
487
488 **MATERIALS AND METHODS**
489
490 **Golden Gate pEAQΔP19 vector construction**
491 Binary vector pEAQΔP19-GG was obtained by, (i) removing 3 SapI restriction sites present
492 in pEAQ-*HT* [56], (ii) inserting a Golden Gate cassette (similar to Gateway without AttR1/2)
493 with SapI sites at extremities and (iii) removing P19. Two silent substitutions into Neomycin
494 phosphotransferase (nptII) gene and one substitution near the origin of replication (ColE1)
495 were produced by PCR mutagenesis using Phusion polymerase in GC buffer supplemented
496 with 5% DMSO (primers in **Supplementary Table 1**, n°595-596 and 638-641) in order to
497 obtain plasmid pEAQ-HT-ΔSapI. A Golden Gate cassette amplicon (pEAQ-HT as matrix, see
498 primer n°589+642 **Supplementary Table 1**) was inserted via AgeI/XhoI restriction sites in
499 pEAQ-HT-ΔSapI. Finally, P19 was excised by double restriction EcoNI/SgsI (FD1304,

500 FD1894, Thermo Scientific), extremities were filled in with Klenow fragment (EP0051,
501 Thermo Scientific), supplemented with dNTPs, followed by a ligation step and
502 transformation in *E. coli* (ccdB Survival strain, Invitrogen).
503
504 **Plant material**
505 Transgenic 35S:*B2:GFP*/*N. benthamiana* plants were previously described [13]. Transgenic
506 *A. thaliana* plants (Col-0 line and genetic backgrounds including mutants of the core antiviral
507 Dicer-Like genes, *dcl2-1*, *dcl4-2* and triple *dcl2-1/dcl3-1/dcl4-2* lines - [30] expressing
508 35S:*B2:GFP* were generated using same plasmid (pEAQΔP19-B2:GFP) and agrobacteria
509 described in [13], following floral dip transformation [57] with addition of PPM (Plant
510 Preservative Mixture, Plant Cell Technology) at 2 ml/L in MS medium. Individual
511 Arabidopsis transformed lines were self-pollinated to generate (F3) plants homozygous for
512 the transgene.
513
514 **Cloning of candidate genes**
515 Candidate genes were amplified from *A. thaliana* genomic DNA with primers designed to
516 contain SapI restriction sites compatible with Golden Gate cloning [58] and adapters
517 necessary for ligation to an N-terminal or C-terminal tag (primer list in **Supplementary**
518 **Table 1**). In the case of genes containing SapI restriction sites, silent mutations were
519 introduced to remove these sites through overlap PCR. In parallel, tRFP was amplified with
520 primers designed to contain SapI restriction sites, adapters for ligation to the N- or C-terminal
521 end of the candidate gene and a peptide linker (GGGSGGG amino acid sequence) between
522 tRFP and the candidate gene. PCR products were purified from agarose gel and used in a
523 Golden Gate reaction containing the candidate gene, tRFP, binary vector pEAQΔP19-GG,
524 SapI (R0569L, New England Biolabs), CutSmart buffer (New England Biolabs), T4 DNA

525 ligase 5U/µl (EL0011, Thermo Scientific) and 0.5 or 1 mM ATP (R0441, Thermo Scientific).
526 Golden Gate reaction cycling: 10 cycles of 37°C 10 min, 18°C 10 min ; 18°C 50 min, 50°C
527 10 min, 80°C 10 min. Following transformation in *E. coli* (TOP10 strain, Invitrogen),
528 purification and sequencing, plasmids were transformed into *A. tumefaciens* strain GV3101.
529 pEAQΔP19-B2:RFP served as matrix to generate plasmid pEAQΔP19-B2mut:RFP as
530 described in [13](primers n°631-632, **Supplementary Table 1**).
531
532 **Plant inoculation and infection**
533 For fluorescence microscopy experiments, leaves of 5-6 week-old 35S:*B2:GFP/N.*
534 *benthamiana* were infiltrated with *A. tumefaciens* GV3101 carrying plasmid pEAQΔP19
535 containing the tagged gene of interest, at absorbance$_{600nm}$ (A_{600}) of 0.2. Prior to inoculation,
536 bacteria were incubated in 10 mM MES pH 5.6, 10 mM $MgCl_2$, 200 µM acetosyringone for 1
537 hour. TRV infection was initiated upon agro-infection with bacteria carrying plasmids
538 expressing the two viral genomic RNAs [24], at A_{600} 0.01 each. This method of virus
539 delivery was chosen because it results in homogenous and ubiquitous infection throughout
540 the inoculated tissue. 3-4 days post-inoculation, leaf disks were collected and observed by
541 confocal microscopy. *A. thaliana* infection was carried out as for *N. benthamiana*, with the
542 difference that *A. tumefaciens* was induced by incubating 5-6 hours in induction medium
543 (10.5 g/L K_2HPO_4, 4.5 g/L KH_2PO_4, 1 g/L $(NH_4)_2SO_4$, 0.5 g/L sodium citrate, 0.1 g/L
544 $MgSO_4$, 0.4% glycerol, 0.1 g/L MES, 200 µM acetosyringone), and bacteria used at A_{600} 0.5
545 each. Systemically infected leaves were harvested 12-13 dpi. *N. benthamiana* plants were
546 kept in a greenhouse at 22-18°C, 16h/8h light/dark photoperiod, while *A. thaliana* were kept
547 in a neon-lit growth chamber at 22-18°C, 12h/12h light/dark photoperiod.
548
549 **Immunoprecipitation**

550 Immunoprecipitations were performed as previously described [22], with minor
551 modifications. 0.15 g of young rosette leaves were ground in liquid nitrogen, homogenized in
552 a chilled mortar with 1 ml lysis buffer (50 mM Tris–HCl, pH 8, 50 mM NaCl, 1% Triton X-
553 100) containing 1 tablet/50 ml of protease inhibitor cocktail (Roche), transferred to a tube and
554 incubated for 15 min at 4°C on a wheel. Cell debris was removed by two successive
555 centrifugations at 12000*g* for 10 min at 4°C, after which an aliquot of supernatant was taken
556 as input fraction. The remaining extract was incubated with magnetic microbeads coated with
557 monoclonal anti-GFP antibodies (µMACS purification system, Miltenyi Biotech, catalog
558 number #130-091-125) at 4°C for 20 min. Sample was then passed through M column
559 (MACS purification system, Miltenyi Biotech) and an aliquot of the flow-through fraction
560 was taken. The M column was then washed 2 times with 500 µl of lysis buffer and 1 time
561 with 100 µl of washing buffer (20 mM Tris–HCl, pH 7.5). The beads and associated immune
562 complexes were recovered by removing the M column from the magnetic stand and passing 1
563 ml Tri Reagent (for subsequent RNA analysis – see dedicated section) or 200 µl hot 1X
564 Laemmli buffer (for protein analysis – see dedicated section). 4X Laemmli buffer was added
565 to input and flow-through fractions before protein denaturation for 5 min at 95°C.
566
567 **RNA extraction and analysis**
568 RNA from total and immunoprecipitated fractions was performed with Tri-Reagent (Sigma)
569 according to manufacturer's instructions. Briefly, 0.2 g tissue were ground in liquid nitrogen
570 and homogenized in 1 ml Tri-Reagent, 400 µl of chloroform were added, and sample was
571 thoroughly shaken for 2 min. After 10 min spin at 13000 rpm, 4°C, supernatant was added to
572 at least 1 vol isopropanol (and 1.5 µl glycogen in the case of immunoprecipitated samples -
573 IP) and incubated 1 hour on ice (O/N for IP). After 15 min spin at 13000 rpm, 4°C (30 min
574 for IP), pellet was washed in 80% ethanol, dried and resuspended in water. RNA was

575 analyzed by northern blot (denaturing agarose gel to detect high molecular weight RNA,
576 denaturing PAGE to detect low molecular weight RNA) and northwestern blot (native
577 agarose gel to detect long double-stranded RNA). In northern blot, miRNA were detected
578 through DNA oligonucleotides labeled with γ-^{32}P-ATP using T4 PNK (see **Supplementary**
579 **Table 1**). TRV genomic and subgenomic RNAs were detected in the same way, with an
580 oligonucleotide complementary to a part of the 3'UTR sequence common to RNA1 and
581 RNA2. TRV-PDS-derived siRNA were detected through PCR-amplified *A. thaliana* PDS
582 sequence labeled by random priming reactions in the presence of α-^{32}P-dCTP. In
583 northwestern blot, dsRNA were detected through recombinant Strep-Tagged FHV B2, as
584 previously described [13].
585
586 **Protein extraction and analysis**
587 Proteins from total fractions were extracted as previously described [59]. Immunoprecipitated
588 proteins for mass spectrometry analysis were isolated as described above, then denatured 5
589 min at 95°C. Immunoprecipitated proteins from RNA IP were obtained by collecting the
590 phenolic phase following Tri-reagent/chloroform extraction, adding 3-4 vol acetone and
591 incubating at -20°C O/N. After centrifugation (13000 rpm, 15 min, 4°C) pellet was washed in
592 80% acetone and resuspended in 1X Laemmli. Proteins were resolved by SDS-PAGE and
593 electro-blotted onto Immobilion-P membrane. This was incubated with the appropriate
594 antibodies (anti-GFP polyclonal antibody and anti-tRFP antibody, Evrogen, reference #
595 AB233) and revealed with Roche LumiLight ECL kit after incubation with secondary
596 antibody.
597
598 **Mass spectrometry analysis and data processing**

599 Proteins were digested with sequencing-grade trypsin (Promega) and analyzed by nanoLC-
600 MS/MS on a TripleTOF 5600 mass spectrometer (Sciex, USA) as described previously [60].
601 Data were searched against the TAIR v.10 database with a decoy strategy (27281 protein
602 forward sequences). Peptides were identified with Mascot algorithm (version 2.5, Matrix
603 Science, London, UK) and data were further imported into Proline v1.4 software
604 (http://proline.profiproteomics.fr/). Proteins were validated on Mascot pretty rank equal to 1,
605 and 1% FDR on both peptide spectrum matches (PSM score) and protein sets (Protein Set
606 score). The total number of MS/MS fragmentation spectra was used to quantify each protein
607 from at least three independent biological replicates. A statistical analysis based on spectral
608 counts was performed using a homemade R package as described in [61]. The R package
609 uses a negative binomial GLM model based on EdgeR [62] and calculates, for each identified
610 protein, a fold-change, a p-value and an adjusted p-value corrected using Benjamini-
611 Hochberg method.
612
613
614 **Confocal laser scanning microscopy**
615 Observations of leaf disks were carried out using Zeiss LSM700 and LSM780 laser scanning
616 confocal microscopes. eGFP was excited at 488 nm, while tRFP was excited at 561 nm.
617 Image processing was performed using ImageJ/FIJI, while figure panels were assembled with
618 Adobe Photoshop.
619
620 **DATA AVAILABILITY**
621 All data are available in the manuscript and in Supplementary files. Raw data from gels and
622 blots can be found with the Blotting Source Data file. Additional confocal acquisitions for
623 each candidate tested can be found in the Microscopy Source Data file. Raw/unprocessed

624 confocal images (.lsm format) and mass spectrometry data used to assemble all figures have
625 been deposited in the public repository Zenodo. They can be accessed at the DOI: TO BE
626 GENERATED.
627

628 **ACKNOWLEDGEMENTS**
629 We thank David Gilmer for providing anti-GFP (Rocco) polyclonal antibodies. Special
630 thanks to Hélène Zuber for the R-script that enabled the statistical analysis of co-IP
631 experiments. We also would like to thank Philippe Hammann for assistance in
632 immunoprecipitation experiments, and Jerome Mutterer and Mathieu Erhardt for assistance in
633 laser confocal microscopy.
634

635 **FUNDING**
636 Funding Disclosure: This work was co-funded by the CNRS and the European Regional
637 Development Fund (ERDF) in the framework of the INTERREG IV and V Upper Rhine
638 programs (BACCHUS and VITIFUTUR projects). B.M. benefited from an IdEx postdoctoral
639 fellowship from the Université de Strasbourg. M.I. also benefited from funds from LABEX:
640 ANR-10-LABX-0036_NETRNA.
641

642 **COMPETING INTERESTS**
643 The authors declare that the research was conducted in the absence of any commercial or
644 financial relationships that could be construed as a potential conflict of interest.
645

646 **AUTHOR CONTRIBUTIONS**
647 Study conception and design: M.I. and C.R.; generation of transgenic *A. thaliana* lines: B.M.;
648 immunoprecipitation experiments: M.I.; RNA and protein extraction, northern and north-

649 western blotting: M.I.; western blotting: M.I. and H.S.; mass spectrometry: L.K.; statistical
650 analysis of co-IP data: L.K. and H.S.; molecular cloning: M.I., B.M. and V.P.; recombinant
651 B2 production: V.P.; *N. benthamiana* inoculation and infection: M.I.; laser confocal
652 microscopy: M.I.; writing: M.I. and C.R.; supervision: C.R.; funding acquisition: C.R. and
653 P.D.
654
655 **FIGURE LEGENDS**
656
657 **Figure 1: Immunoprecipitation of B2:GFP allows the isolation of TRV dsRNA *in vivo*.**
658 **(A)** Photos of *A. thaliana* Col-0 and 35S:*B2:GFP*/Col-0 plants 13 days post-infection with
659 TRV-PDS. **(B)** Confocal microscopy analysis of non-infected (n.i. - top left) and TRV-PDS
660 systemically-infected leaves of 35S:*B2:GFP*/Col-0 plants. On the right, higher magnification
661 (63x) images of TRV replication complexes from the same tissues as those visible at lower
662 magnification (20x) on the left middle and bottom. **(C)** Northern blot analysis of high
663 molecular weight RNA from total fractions of TRV-PDS-infected wild-type or 35S:*B2:GFP*
664 *N. benthamiana* (left), and from total (middle) and anti-GFP immunoprecipitated (right)
665 fractions from infected 35S:*GFP* and 35S:*B2:GFP/*Col-0 *A. thaliana*. **(D)** Northwestern blot
666 analysis of native-state high molecular weight RNA from samples described in (C). EtBr
667 staining was used as loading control in (C) and (D). **(E)** Northern blot analysis of low
668 molecular weight RNA from samples described in (C). The probes were applied sequentially
669 on the same membrane in successive rounds of probing and stripping. snU6 and miR159
670 were used as loading controls. **(F)** Western blot analysis of proteins from the same
671 immunoprecipitation experiment analyzed in (C). Coomassie staining was used as loading
672 control. Source data is available with the Blotting Source Data.
673

674 **Figure 2: Immunoprecipitation of B2:GFP allows the isolation of TRV proteins and**
675 **host factors.** Mass spectrometry analyses of anti-GFP immunoprecipitated proteins from
676 TRV-PDS-infected 35S:*GFP*/Col-0 and 35S:*B2:GFP*/Col-0 plants. Three technical replicates
677 were performed and analyzed per genotype. *A. thaliana* proteins shown here are the ones that
678 have been tested in this study. Abbreviations correspond to those available in literature,
679 except for RP27a and RUP1, which have been here assigned for lack of previously
680 established ones. Accession numbers correspond to UniProt (TRV proteins) and TAIR (*A.*
681 *thaliana* proteins) databases. **(A)** Table containing the spectral counts obtained per technical
682 replicate for bait proteins (GFP + B2), TRV proteins and *A. thaliana* proteins. **(B)** Volcano
683 plot representation shows the enrichment of proteins from TRV-infected plants that co-
684 purified with B2:GFP. Y- and X-axis display adjusted p-values and fold changes,
685 respectively. The dashed line indicates the threshold above which proteins are significantly
686 enriched (adjP < 0.05). The source data are available in **Supplementary Table 2**, **(C)**
687 Sequence coverage obtained on all the proteins listed in (A). For each of the 14 entries, the
688 length of the protein is displayed while the covered residues are highlighted with blue vertical
689 bars. The total number of spectra matching on each protein in the three replicates is indicated,
690 as well as the corresponding total number of unique peptide sequences. The complete protein
691 list can be found in Supplementary Table 2.
692
693 **Figure 3: tRFP does not re-localize to TRV replication complexes.** Laser confocal
694 microscopy on 35S:*B2:GFP/N. benthamiana* leaves transiently expressing 35S:*tRFP*. **(A)**
695 Acquisition from non-infected leaf disks (20x objective). Scale bars indicate 50 µm. **(B)**
696 Acquisition of TRV-PDS-infected leaf disks (20x objective, top), focused on TRV replication
697 complexes (63x objective, middle and bottom). Scale bars indicate 50 and 10 µm,
698 respectively. Additional acquisitions can be found with the Microscopy Source Data.

699

700 **Figure 4: *A. thaliana* double-stranded RNA-binding proteins localize at TRV replication**
701 **complexes. (A)** Summary of mass spectrometry data obtained on DRB2 and DRB4, as a
702 volcano plot (left) and sequence coverage plot (right), already shown in Figure 1. **(B-D)**
703 Laser confocal microscopy on 35S:*B2:GFP/N. benthamiana* leaves transiently expressing
704 35S:*DRB2:tRFP* (B,C) or 35S:*DRB4:tRFP* (D,E). **(B)** Acquisitions with 20x objective of
705 non-infected (top) and TRV-PDS-infected (bottom) leaf disks expressing DRB2:tRFP. Scale
706 bars indicate 50 µm. **(C)** Acquisitions with 63x objective of TRV-PDS-infected leaf disks of
707 tissue described in (B). Scale bars indicate 10 µm. **(D,E)** As in (B,C), but from tissue
708 expressing DRB4:tRFP. Additional acquisitions can be found with the Microscopy Source
709 Data.

710

711

712 **Figure 5: Proteins previously implicated in viral life cycle localize at or near the**
713 **replication complexes. (A)** Summary of mass spectrometry data obtained on HSP70,
714 HSP70-1, HSP70-3 and BTR1, as a volcano plot (left) and sequence coverage plot (right),
715 already shown in Figure 1. **(B-E)** Laser confocal microscopy on 35S:*B2:GFP/N.*
716 *benthamiana* TRV-PDS-infected leaf disks transiently expressing **(A)** 35S:*HSP70:tRFP,* **(B)**
717 35S:*HSP70-1:tRFP*, **(C)** 35S:*HSP70-3:tRFP,* **(D)** 35S:*BTR1:tRFP*. Acquisitions in (B): 20x
718 objective, scale bars indicate 50 µm. Acquisitions in (C, D, E): 63x objective, scale bars
719 indicate 10 µm. Additional acquisitions can be found with the Microscopy Source Data.

720

721

722

723 **Figure 6: Localization of previously undescribed proteins at or near the replication**
724 **complexes. (A)** Summary of mass spectrometry data obtained on RUP1, RP27a and NFD2,
725 as a volcano plot (left) and sequence coverage plot (right), already shown in Figure 1. Laser
726 confocal microscopy (63x objective) on 35S:*B2:GFP/N. benthamiana* TRV-PDS-infected
727 leaf disks transiently expressing **(A)** 35S:*RUP1:tRFP*, **(B)** 35S:*tRFP:RP27a*, **(C)**
728 35S:*tRFP:NFD2*. Scale bars indicate 10 µm. Additional acquisitions can be found with the
729 Microscopy Source Data.
730
731 **Supplementary Figure 1: (A)** Western blot analysis to detect GFP in protein extracts from
732 35S:*B2:GFP* transgenic *A. thaliana* lines in Col-0 and *dcl2-1*, *dcl4-2* and triple *dcl2-1/dcl3-*
733 *1/dcl4-2* mutant backgrounds. Coomassie blue was used as loading control. **(B)** Northern
734 analysis of low molecular weight RNA (PAGE gel) from the plants described in (A), to
735 detect endogenous miRNA (miR159, miR160) and siRNA (TAS1, IR71). Probes were
736 hybridized to the membrane through sequential stripping and probing. **(C)** Photos of the
737 plants described in (A). **(D)** *N. benthamiana* leaf infiltrated with *A. tumefaciens* expressing
738 GFP alone (top left) or in combination with P38, B2:tRFP or B2mut:tRFP, and illuminated
739 with UV light. **(E)** Western blot analysis to detect GFP (top) and tRFP (bottom) in protein
740 extracts from the infiltrated patches described in (E). **(F)** Northern analysis of high molecular
741 weight RNA (agarose gel) from TRV-PDS systemically infected Col-0 and *dcl* mutant
742 backgrounds. Source data is available with the Blotting Source Data.
743
744 **Supplementary Figure 2:** Western analysis to detect GFP in protein extracts from the input,
745 flow-through and anti-GFP immunoprecipitated fractions obtained from TRV-PDS-infected
746 35S:*GFP*/Col-0 and 35S:*B2:GFP*/Col-0 plants, performed in three technical replicates.
747 Coomassie staining was used as loading control. The proteins from the immunoprecipitated

748 fraction were further analyzed by mass spectrometry, and the results are shown in Table 1.
749 Source data is available with the Blotting Source Data.
750
751 **Supplementary Figure 3:** Laser confocal microscopy (20x objective) on 35S:*B2:GFP/N.*
752 *benthamiana* non-infected (left) and TRV-PDS-infected (right) leaf disks transiently
753 expressing **(A)** 35S:*HSP70:tRFP,* **(B)** 35S:*HSP70-1:tRFP*, **(C)** 35S:*HSP70-3:tRFP*, **(D)**
754 35S:*BTR1:tRFP*. Scale bars indicate 50µm. Additional acquisitions can be found with the
755 Microscopy Source Data in the Supplementary Information.
756
757
758 **Supplementary Figure 4:** Laser confocal microscopy (20x objective) on 35S:*B2:GFP/N.*
759 *benthamiana* non-infected (left) and TRV-PDS-infected (right) leaf disks transiently
760 expressing **(A)** 35S:*RUP1:tRFP,* **(B)** 35S:*tRFP:RP27a*, **(C)** 35S:*tRFP:NFD2*. Scale bars
761 indicate 50µm. Additional acquisitions can be found with the Microscopy Source Data in the
762 Supplementary Information.
763
764 **Supplementary Figure 5: (A)** Sequence coverage obtained by MS on the RP27a protein
765 (P59271). Four distinct tryptic peptides have been validated by Mascot algorithm at
766 FDR<1% (bold residues). The total number of spectra matching on the 4 peptides are
767 displayed as green bars with a color code according to the replicate. The Ubiquitin domain
768 [1-76] is highlighted in green. Tryptic cleavage sites (K/R) are underlined. **(B)** Multiple
769 sequence alignment between RP27a sequence and UBQ1 to UBQ14 *A.thaliana* sequences
770 (UniProtKB). Output generated with the MUSCLE tool
771 (https://www.ebi.ac.uk/Tools/msa/muscle). **(C)** MS/MS spectrum corresponding to the
772 ubiquitinated peptide [43-54] LIFAGK(Ub)QLEDGR identified by Mascot algorithm on

773 RP27a protein (Score = 55.68, m/z=487.60, 3+, RT=42.97min). The fragmentation pattern
774 involving the y- and b-ions validated by Mascot is displayed on the upper left corner. The di-
775 glycine motif is highlighted by the GL abbreviation above the K-48 residue, as well as the
776 mass difference between y(6) and y(7) fragments.
777
778 **REFERENCES**

779 1. Grangeon R, Jiang J, Laliberté JF. Host endomembrane recruitment for plant RNA
780 virus replication. Curr Opin Virol. 2012;2(6):683-90. doi: 10.1016/j.coviro.2012.10.003.
781 2. Laliberté JF, Zheng H. Viral Manipulation of Plant Host Membranes. Annu Rev
782 Virol. 2014;1(1):237-59. doi: 10.1146/annurev-virology-031413-085532.
783 3. Ritzenthaler C, Elamawi R. The ER in replication of positive-strand RNA viruses. In
784 Plant Cell Monogr., The Plant Endoplasmic Reticulum. ed. D.G. Robinson Springer; 2006. p.
785 309-30.
786 4. Verchot J. Wrapping membranes around plant virus infection. Curr Opin Virol.
787 2011;1(5):388-95. doi: 10.1016/j.coviro.2011.09.009.
788 5. Nagy PD. Tombusvirus-Host Interactions: Co-Opted Evolutionarily Conserved Host
789 Factors Take Center Court. Annu Rev Virol. 2016;3(1):491-515. doi: 10.1146/annurev-
790 virology-110615-042312.
791 6. Nagy PD, Pogany J. The dependence of viral RNA replication on co-opted host
792 factors. Nature Reviews Microbiology. 2012;10(2):137.
793 7. Wang A. Dissecting the molecular network of virus-plant interactions: the complex
794 roles of host factors. Annu Rev Phytopathol. 2015;53:45-66. doi: 10.1146/annurev-phyto-
795 080614-120001.

796 8. Barton DA, Roovers EF, Gouil Q, da Fonseca GC, Reis RS, Jackson C, et al. Live
797 Cell Imaging Reveals the Relocation of dsRNA Binding Proteins Upon Viral Infection.
798 Molecular plant-microbe interactions. 2017;30(6):435-43.
799 9. Guo Z, Li Y, Ding SW. Small RNA-based antimicrobial immunity. Nat Rev
800 Immunol. 2019;19(1):31-44. doi: 10.1038/s41577-018-0071-x.
801 10. Incarbone M, Dunoyer P. RNA silencing and its suppression: novel insights from in
802 planta analyses. Trends Plant Sci. 2013;18(7):382-92. doi: 10.1016/j.tplants.2013.04.001.
803 11. Elvira-Matelot E, Hachet M, Shamandi N, Comella P, Saez-Vasquez J, Zytnicki M, et
804 al. Arabidopsis RNASE THREE LIKE2 modulates the expression of protein-coding genes
805 via 24-nt siRNA-directed DNA methylation. The Plant Cell. 2016:TPC2015-00540-RA.
806 12. Shamandi N, Zytnicki M, Charbonnel C, Elvira-Matelot E, Bochnakian A, Comella P,
807 et al. Plants encode a general siRNA suppressor that is induced and suppressed by viruses.
808 PLoS biology. 2015;13(12):e1002326.
809 13. Monsion B, Incarbone M, Hleibieh K, Poignavent V, Ghannam A, Dunoyer P, et al.
810 Efficient detection of long dsRNA in vitro and in vivo using the dsRNA binding domain from
811 FHV B2 protein. Frontiers in plant science. 2018;9:70.
812 14. Cheng X, Deng P, Cui H, Wang A. Visualizing double-stranded RNA distribution and
813 dynamics in living cells by dsRNA binding-dependent fluorescence complementation.
814 Virology. 2015;485:439-51. doi: 10.1016/j.virol.2015.08.023.
815 15. Li Y, Xiong R, Bernards M, Wang A. Recruitment of Arabidopsis RNA Helicase
816 AtRH9 to the Viral Replication Complex by Viral Replicase to Promote Turnip Mosaic Virus
817 Replication. Sci Rep. 2016;6:30297. doi: 10.1038/srep30297.
818 16. Wei T, Zhang C, Hou X, Sanfaçon H, Wang A. The SNARE protein Syp71 is
819 essential for turnip mosaic virus infection by mediating fusion of virus-induced vesicles with
820 chloroplasts. PLoS pathogens. 2013;9(5):e1003378.

821 17. Dufresne PJ, Thivierge K, Cotton S, Beauchemin C, Ide C, Ubalijoro E, et al. Heat
822 shock 70 protein interaction with Turnip mosaic virus RNA-dependent RNA polymerase
823 within virus-induced membrane vesicles. Virology. 2008;374(1):217-27.
824 18. Lohmus A, Varjosalo M, Makinen K. Protein composition of 6K2-induced membrane
825 structures formed during Potato virus A infection. Mol Plant Pathol. 2016;17(6):943-58. doi:
826 10.1111/mpp.12341.
827 19. Wang X, Cao X, Liu M, Zhang R, Zhang X, Gao Z, et al. Hsc70-2 is required for Beet
828 black scorch virus infection through interaction with replication and capsid proteins.
829 Scientific reports. 2018;8(1):4526.
830 20. Merzlyak EM, Goedhart J, Shcherbo D, Bulina ME, Shcheglov AS, Fradkov AF, et
831 al. Bright monomeric red fluorescent protein with an extended fluorescence lifetime. Nature
832 methods. 2007;4(7):555.
833 21. Pumplin N, Voinnet O. RNA silencing suppression by plant pathogens: defence,
834 counter-defence and counter-counter-defence. Nat Rev Microbiol. 2013;11(11):745-60. doi:
835 10.1038/nrmicro3120.
836 22. Incarbone M, Zimmermann A, Hammann P, Erhardt M, Michel F, Dunoyer P.
837 Neutralization of mobile antiviral small RNA through peroxisomal import. Nature plants.
838 2017;3(7):17094.
839 23. Kasschau KD, Xie Z, Allen E, Llave C, Chapman EJ, Krizan KA, et al. P1/HC-Pro, a
840 viral suppressor of RNA silencing, interferes with Arabidopsis development and miRNA
841 function. Developmental cell. 2003;4(2):205-17.
842 24. Li H, Li WX, Ding SW. Induction and suppression of RNA silencing by an animal
843 virus. Science. 2002;296(5571):1319-21. doi: 10.1126/science.1070948.

844 25. Seo J-K, Kwon S-J, Rao A. Molecular dissection of Flock house virus protein B2
845 reveals that electrostatic interactions between N-terminal domains of B2 monomers are
846 critical for dimerization. Virology. 2012;432(2):296-305.
847 26. Chao JA, Lee JH, Chapados BR, Debler EW, Schneemann A, Williamson JR. Dual
848 modes of RNA-silencing suppression by Flock House virus protein B2. Nat Struct Mol Biol.
849 2005;12(11):952-7. doi: 10.1038/nsmb1005.
850 27. Qi N, Zhang L, Qiu Y, Wang Z, Si J, Liu Y, et al. Targeting of dicer-2 and RNA by a
851 viral RNA silencing suppressor in Drosophila cells. J Virol. 2012;86(10):5763-73. doi:
852 10.1128/JVI.07229-11.
853 28. Singh G, Popli S, Hari Y, Malhotra P, Mukherjee S, Bhatnagar RK. Suppression of
854 RNA silencing by Flock house virus B2 protein is mediated through its interaction with the
855 PAZ domain of Dicer. The FASEB Journal. 2009;23(6):1845-57.
856 29. Liu Y, Schiff M, Dinesh-Kumar SP. Virus-induced gene silencing in tomato. Plant J.
857 2002;31(6):777-86. doi: 10.1046/j.1365-313x.2002.01394.x.
858 30. Deleris A, Gallego-Bartolome J, Bao J, Kasschau KD, Carrington JC, Voinnet O.
859 Hierarchical action and inhibition of plant Dicer-like proteins in antiviral defense. Science.
860 2006;313(5783):68-71. doi: 10.1126/science.1128214.
861 31. Fujisaki K, Ishikawa M. Identification of an Arabidopsis thaliana protein that binds to
862 tomato mosaic virus genomic RNA and inhibits its multiplication. Virology.
863 2008;380(2):402-11.
864 32. Clavel M, Pelissier T, Descombin J, Jean V, Picart C, Charbonel C, et al. Parallel
865 action of AtDRB2 and RdDM in the control of transposable element expression. BMC Plant
866 Biol. 2015;15(1):70. doi: 10.1186/s12870-015-0455-z.
867 33. Bhat R, Vyas D. Myrosinase: insights on structural, catalytic, regulatory, and
868 environmental interactions. Critical reviews in biotechnology. 2019;39(4):508-23.

869 34. Otulak K, Chouda M, Bujarski J, Garbaczewska G. The evidence of Tobacco rattle
870 virus impact on host plant organelles ultrastructure. Micron. 2015;70:7-20. doi:
871 10.1016/j.micron.2014.11.007.
872 35. Schauer SE, Jacobsen SE, Meinke DW, Ray A. DICER-LIKE1: blind men and
873 elephants in Arabidopsis development. Trends Plant Sci. 2002;7(11):487-91.
874 36. Tschopp M-A, Iki T, Brosnan CA, Jullien PE, Pumplin N. A complex of Arabidopsis
875 DRB proteins can impair dsRNA processing. RNA. 2017;23(5):782-97.
876 37. Eamens AL, Wook Kim K, Waterhouse PM. DRB2, DRB3 and DRB5 function in a
877 non-canonical microRNA pathway in Arabidopsis thaliana. Plant Signal Behav.
878 2012;7(10):1224-9. doi: 10.4161/psb.21518.
879 38. Pélissier T, Clavel M, Chaparro C, Pouch-Pélissier M-N, Vaucheret H, Deragon J-M.
880 Double-stranded RNA binding proteins DRB2 and DRB4 have an antagonistic impact on
881 polymerase IV-dependent siRNA levels in Arabidopsis. RNA. 2011;17(8):1502-10.
882 39. Fukudome A, Kanaya A, Egami M, Nakazawa Y, Hiraguri A, Moriyama H, et al.
883 Specific requirement of DRB4, a dsRNA-binding protein, for the in vitro dsRNA-cleaving
884 activity of Arabidopsis Dicer-like 4. RNA. 2011;17(4):750-60. doi: 10.1261/rna.2455411.
885 40. Montavon T, Kwon Y, Zimmermann A, Hammann P, Vincent T, Cognat V, et al. A
886 specific dsRNA-binding protein complex selectively sequesters endogenous inverted-repeat
887 siRNA precursors and inhibits their processing. Nucleic acids research. 2017;45(3):1330-44.
888 41. Jakubiec A, Yang SW, Chua NH. Arabidopsis DRB4 protein in antiviral defense
889 against Turnip yellow mosaic virus infection. Plant J. 2012;69(1):14-25. doi: 10.1111/j.1365-
890 313X.2011.04765.x.
891 42. Qu F, Ye X, Morris TJ. Arabidopsis DRB4, AGO1, AGO7, and RDR6 participate in a
892 DCL4-initiated antiviral RNA silencing pathway negatively regulated by DCL1. Proceedings
893 of the National Academy of Sciences. 2008;105(38):14732-7.

894 43. Verchot J. Cellular chaperones and folding enzymes are vital contributors to
895 membrane bound replication and movement complexes during plant RNA virus infection.
896 Front Plant Sci. 2012;3:275. doi: 10.3389/fpls.2012.00275.
897 44. Lõhmus A, Hafrén A, Mäkinen K. Coat protein regulation by CK2, CPIP, HSP70, and
898 CHIP is required for Potato virus A replication and coat protein accumulation. Journal of
899 virology. 2017;91(3):e01316-16.
900 45. Pogany J, Nagy PD. Activation of Tomato bushy stunt virus RNA-dependent RNA
901 polymerase by cellular heat shock protein 70 is enhanced by phospholipids in vitro. Journal
902 of virology. 2015;89(10):5714-23.
903 46. Yang J, Zhang F, Cai NJ, Wu N, Chen X, Li J, et al. A furoviral replicase recruits host
904 HSP70 to membranes for viral RNA replication. Sci Rep. 2017;7:45590. doi:
905 10.1038/srep45590.
906 47. Portereiko MF, Sandaklie-Nikolova L, Lloyd A, Dever CA, Otsuga D, Drews GN.
907 NUCLEAR FUSION DEFECTIVE1 encodes the Arabidopsis RPL21M protein and is
908 required for karyogamy during female gametophyte development and fertilization. Plant
909 physiology. 2006;141(3):957-65.
910 48. Nishikiori M, Dohi K, Mori M, Meshi T, Naito S, Ishikawa M. Membrane-bound
911 tomato mosaic virus replication proteins participate in RNA synthesis and are associated with
912 host proteins in a pattern distinct from those that are not membrane bound. Journal of
913 virology. 2006;80(17):8459-68.
914 49. Serva S, Nagy PD. Proteomics analysis of the tombusvirus replicase: Hsp70
915 molecular chaperone is associated with the replicase and enhances viral RNA replication.
916 Journal of virology. 2006;80(5):2162-9.

917 50. Kobayashi K, Tomita R, Sakamoto M. Recombinant plant dsRNA-binding protein as
918 an effective tool for the isolation of viral replicative form dsRNA and universal detection of
919 RNA viruses. Journal of general plant pathology. 2009;75(2):87.
920 51. de Castro IF, Fernández JJ, Barajas D, Nagy PD, Risco C. Three-dimensional imaging
921 of the intracellular assembly of a functional viral RNA replicase complex. J Cell Sci.
922 2017;130(1):260-8.
923 52. Nagy PD, Strating JR, van Kuppeveld FJ. Building Viral Replication Organelles:
924 Close Encounters of the Membrane Types. PLoS Pathog. 2016;12(10):e1005912. doi:
925 10.1371/journal.ppat.1005912.
926 53. Romero-Brey I, Bartenschlager R. Membranous replication factories induced by plus-
927 strand RNA viruses. Viruses. 2014;6(7):2826-57. doi: 10.3390/v6072826.
928 54. Alcaide-Loridan C, Jupin I. Ubiquitin and plant viruses, let's play together! Plant
929 Physiol. 2012;160(1):72-82. doi: 10.1104/pp.112.201905.
930 55. Verchot J. Plant Virus Infection and the Ubiquitin Proteasome Machinery: Arms Race
931 along the Endoplasmic Reticulum. Viruses. 2016;8(11):314. doi: 10.3390/v8110314.
932 56. Sainsbury F, Thuenemann EC, Lomonossoff GP. pEAQ: versatile expression vectors
933 for easy and quick transient expression of heterologous proteins in plants. Plant Biotechnol J.
934 2009;7(7):682-93. doi: 10.1111/j.1467-7652.2009.00434.x.
935 57. Harrison SJ, Mott EK, Parsley K, Aspinall S, Gray JC, Cottage A. A rapid and robust
936 method of identifying transformed Arabidopsis thaliana seedlings following floral dip
937 transformation. Plant Methods. 2006;2(1):19. doi: 10.1186/1746-4811-2-19.
938 58. Engler C, Gruetzner R, Kandzia R, Marillonnet S. Golden gate shuffling: a one-pot
939 DNA shuffling method based on type IIs restriction enzymes. PLoS One. 2009;4(5):e5553.
940 doi: 10.1371/journal.pone.0005553.

941 59. Hurkman WJ, Tanaka CK. Solubilization of plant membrane proteins for analysis by
942 two-dimensional gel electrophoresis. Plant Physiol. 1986;81(3):802-6. doi:
943 10.1104/pp.81.3.802.
944 60. Chicher J, Simonetti A, Kuhn L, Schaeffer L, Hammann P, Eriani G, et al.
945 Purification of mRNA-programmed translation initiation complexes suitable for mass
946 spectrometry analysis. Proteomics. 2015;15(14):2417-25.
947 61. Lange H, Ndecky SYA, Gomez-Diaz C, Pflieger D, Butel N, Zumsteg J, et al. RST1
948 and RIPR connect the cytosolic RNA exosome to the Ski complex in Arabidopsis. Nature
949 Communications. 2019;10(1):3871. doi: 10.1038/s41467-019-11807-4.
950 62. Robinson MD, McCarthy DJ, Smyth GK. edgeR: a Bioconductor package for
951 differential expression analysis of digital gene expression data. Bioinformatics.
952 2010;26(1):139-40. doi: 10.1093/bioinformatics/btp616.
953

Figure 1

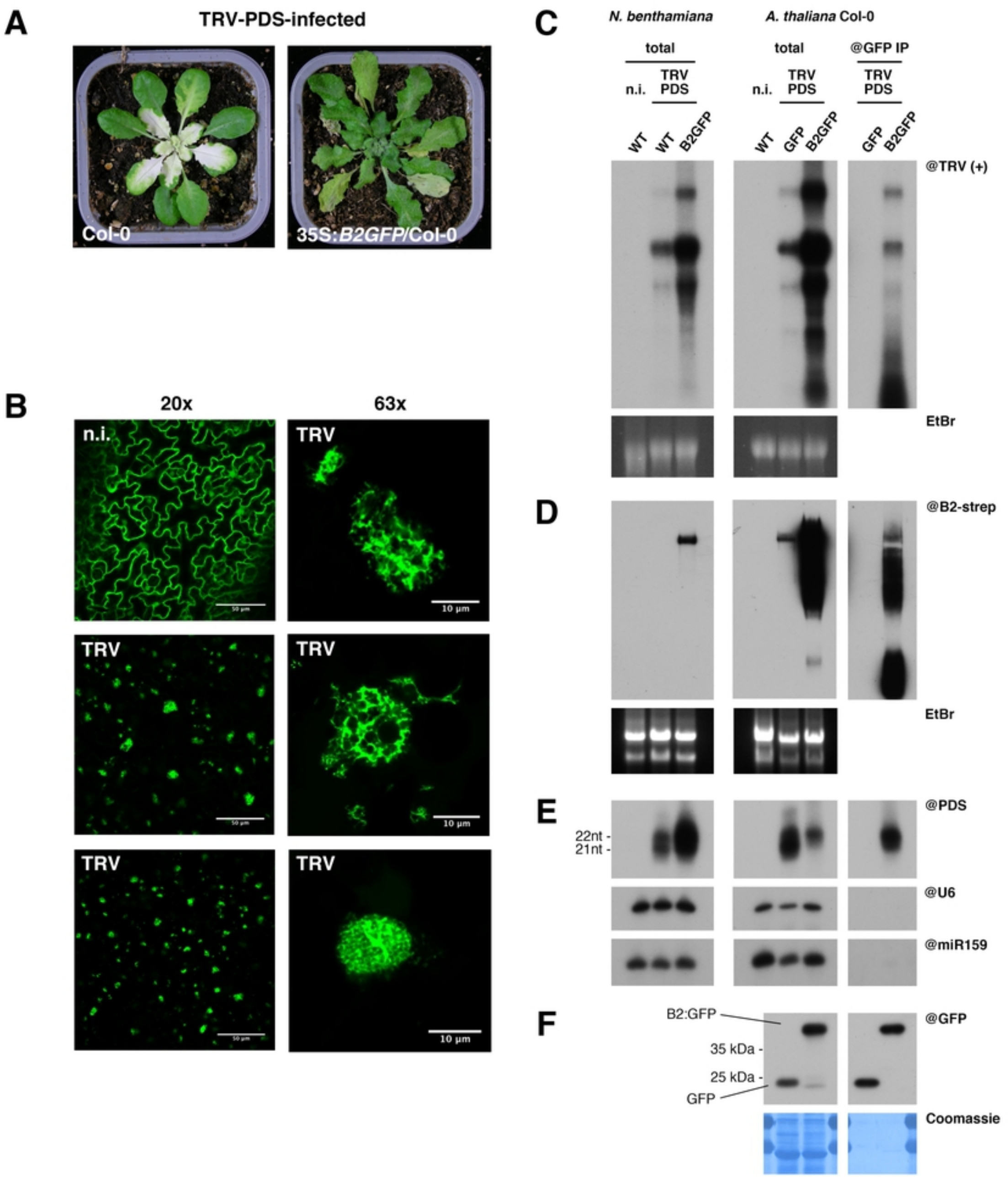
A
TRV-PDS-infected
Col-0
35S:B2GFP/Col-0
B
20x
63x
n.i.
TRV
TRV
TRV
TRV
TRV
10 µm
C
N. benthamiana
A. thaliana Col-0
total
total
@GFP IP
n.i.
TRV PDS
WT
WT
B2GFP
GFP
@TRV (+)
EtBr
D
@B2-strep
E
@PDS
22nt -
21nt -
@U6
@miR159
F
B2:GFP
@GFP
35 kDa -
25 kDa -
GFP
Coomassie

Figure 2

A

Description	Abbreviation	Accession	Spectral count					
			35S:*GFP*/Col-0			35S:*B2GFP*/Col-0		
			#1	#2	#3	#1	#2	#3
GFP			425	504	676	871	1042	963
B2			4			878	806	883
TRV Replicase		Q9J942				203	219	220
TRV Coat Protein		Q88897				249	250	250
TRV 16k Protein		Q77JX3				6	8	5
Ribosomal protein S27a	RP27a	AT1G23410				27	29	26
Heat Shock Protein 70-1	HSP70-1	AT5G02500				24	29	28
Heat Shock Protein 70-3	HSP70-3	AT3G09440				22	26	23
Heat Shock Protein 70	HSP70	AT3G12580				18	23	22
RING/U-box Protein	RUP1	AT3G45570				17	19	14
Ribonuclease III family protein	NFD2	AT1G24450				2	4	6
Binding to ToMV RNA 1	BTR1	AT5G04430				2	4	1
DsRNA-binding Protein 4	DRB4	AT3G62800				2	2	1
DsRNA-binding Protein 2	DRB2	AT2G28380					1	3

B

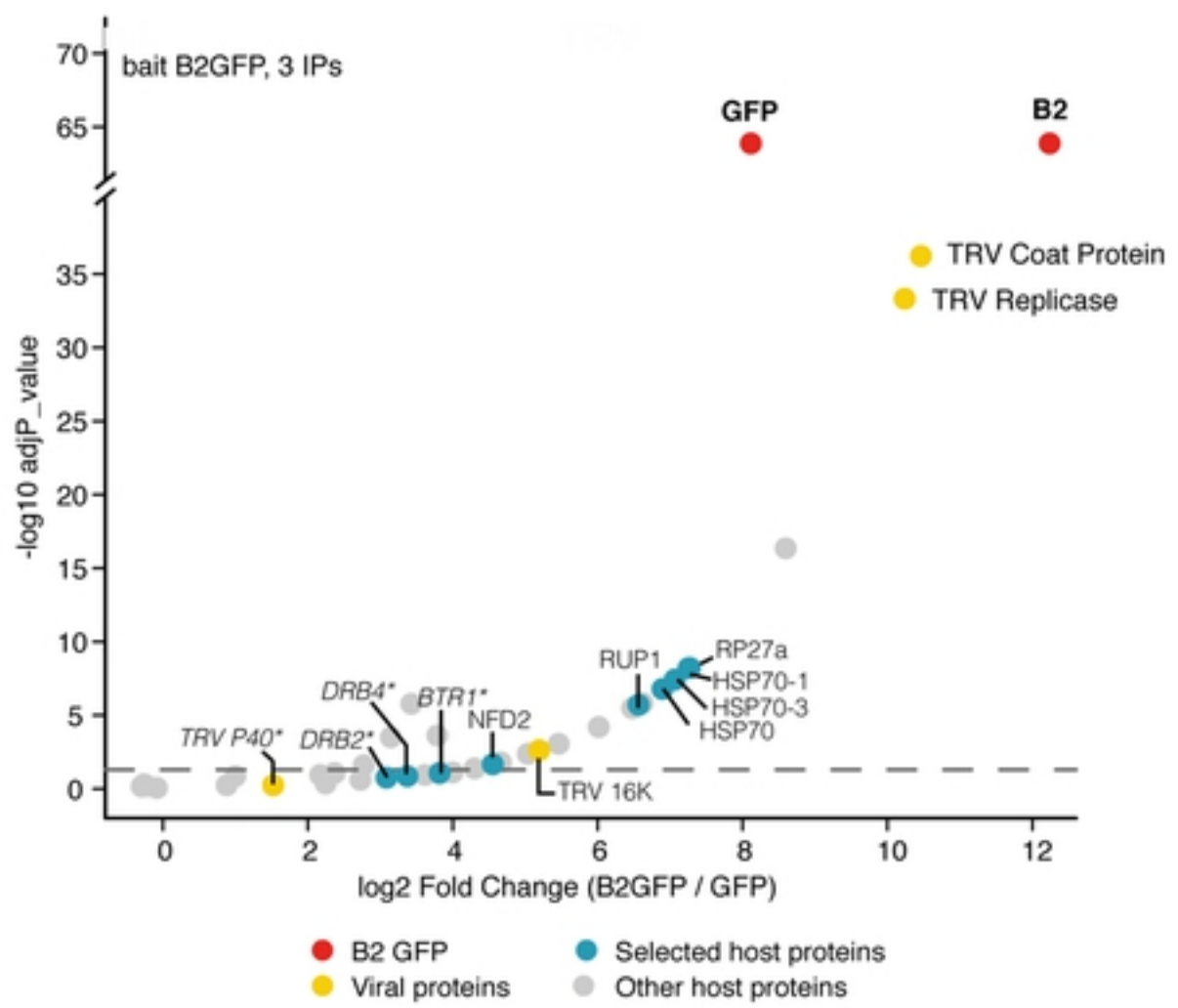

C

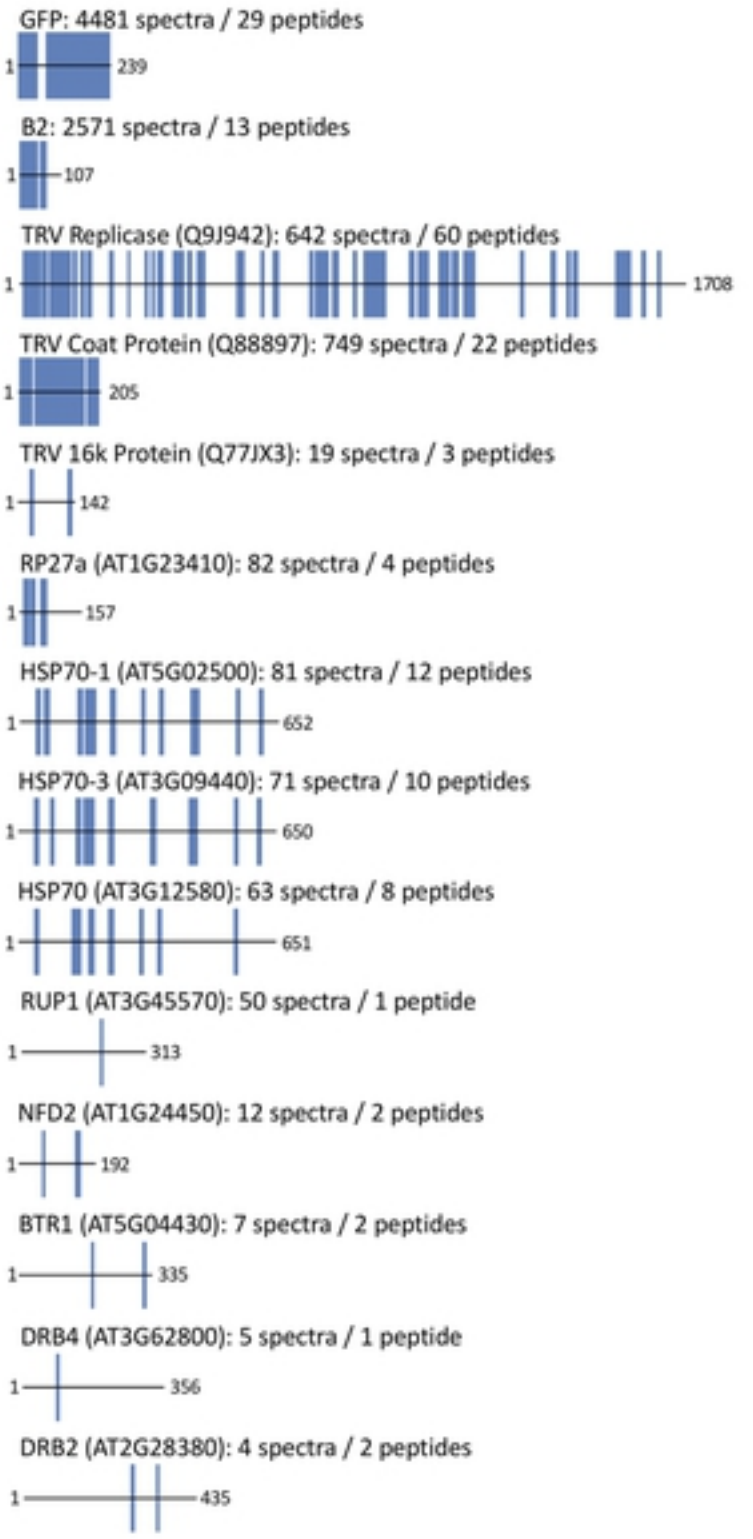

Figure 3

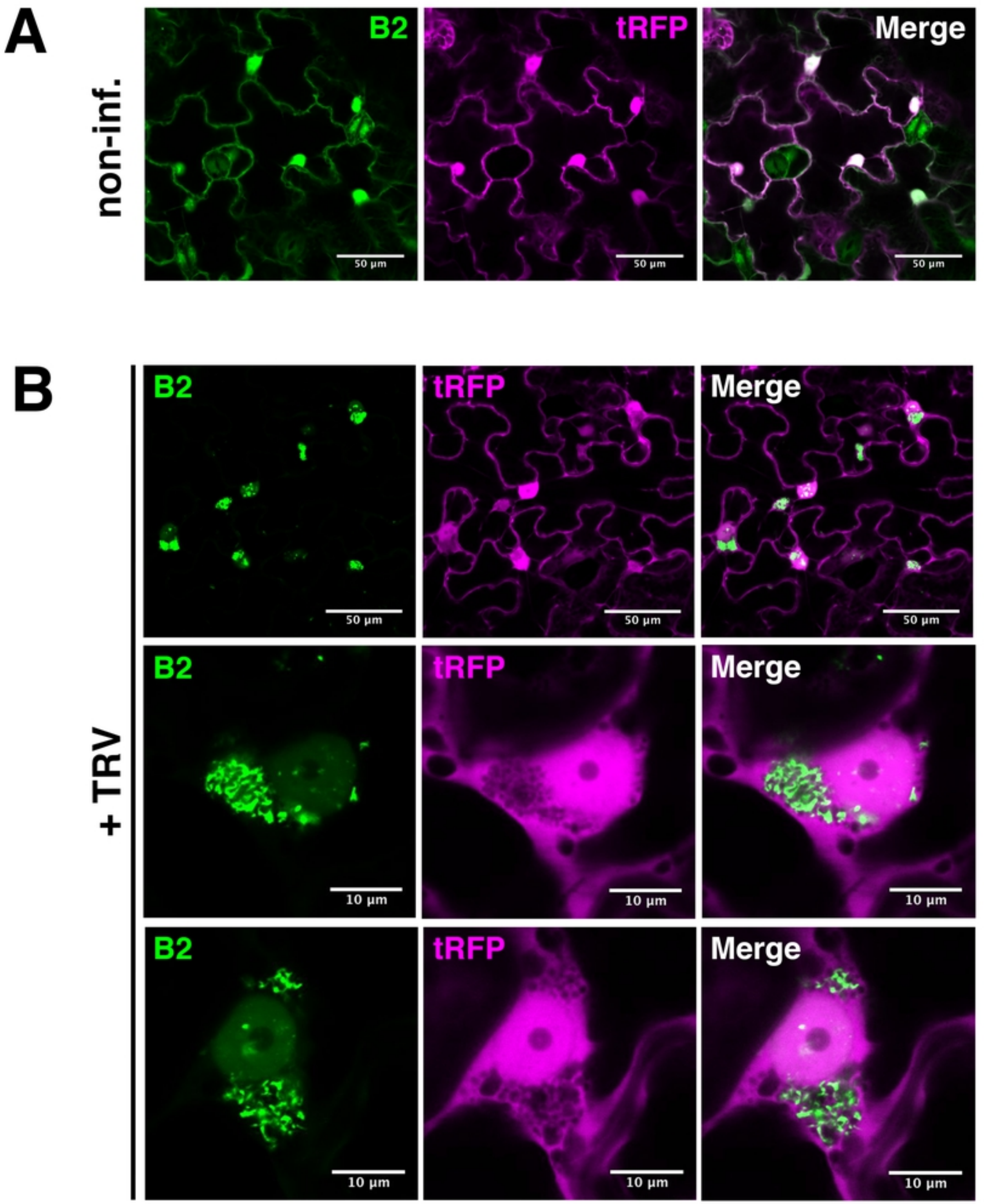

Figure 4

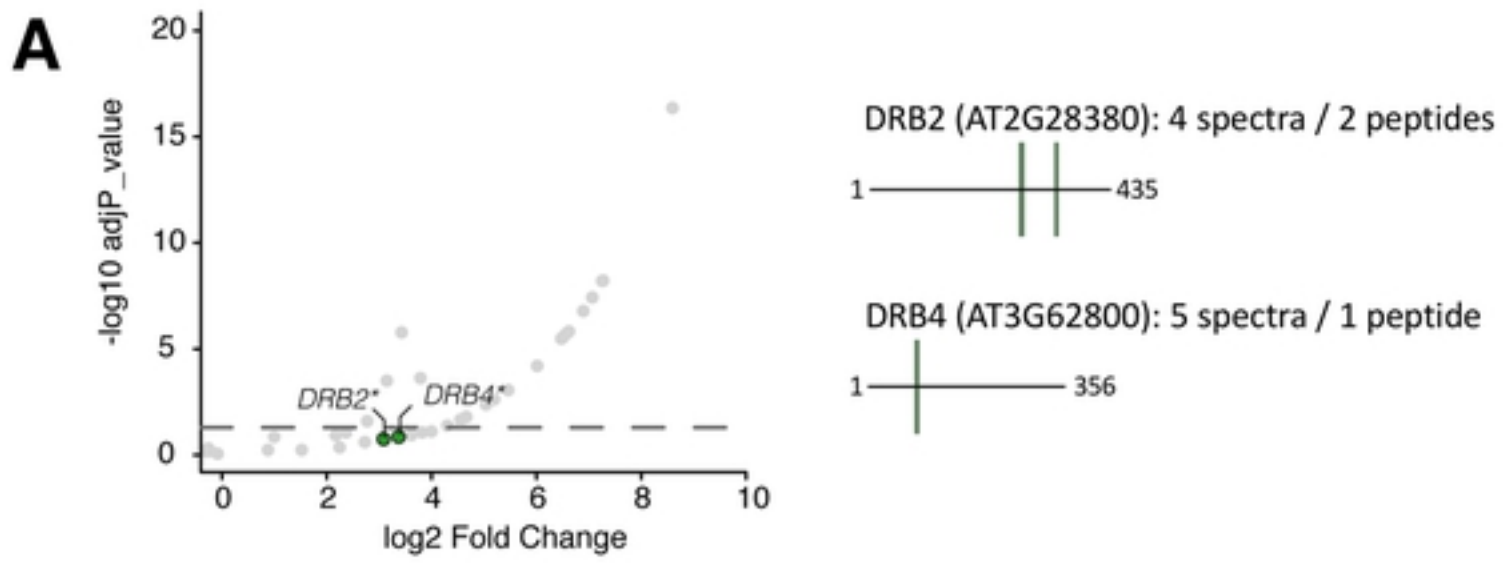
A
-log10 adjP_value
log2 Fold Change
DRB2*
DRB4*
DRB2 (AT2G28380): 4 spectra / 2 peptides
1
435
DRB4 (AT3G62800): 5 spectra / 1 peptide
1
356

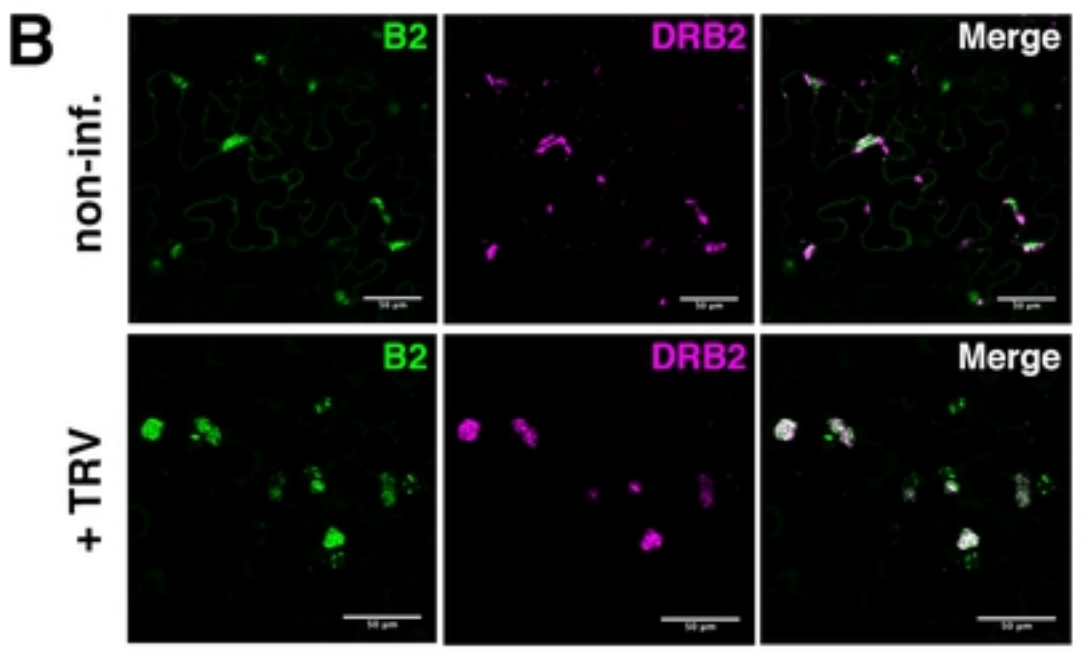
B
non-inf.
+ TRV
B2
DRB2
Merge

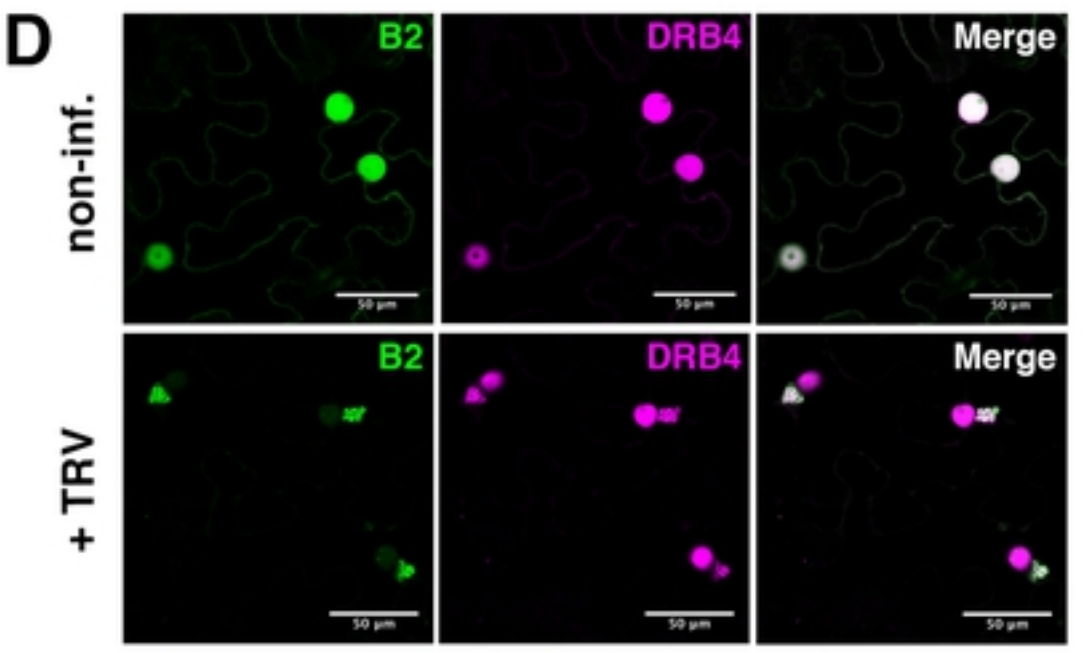
D
non-inf.
+ TRV
B2
DRB4
Merge

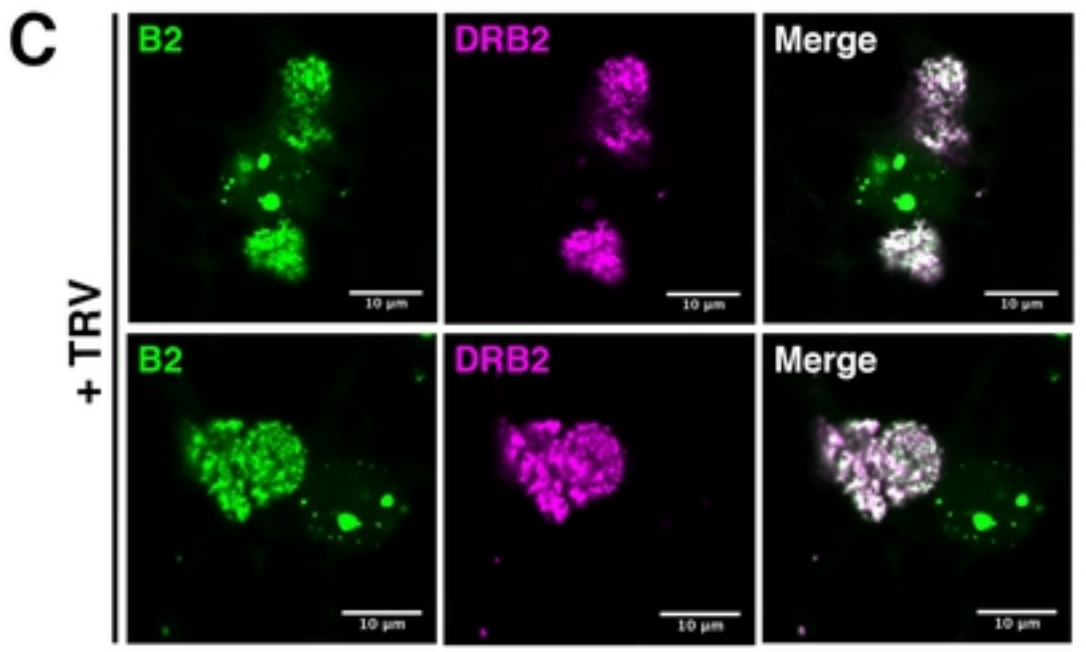
C
+ TRV
B2
DRB2
Merge

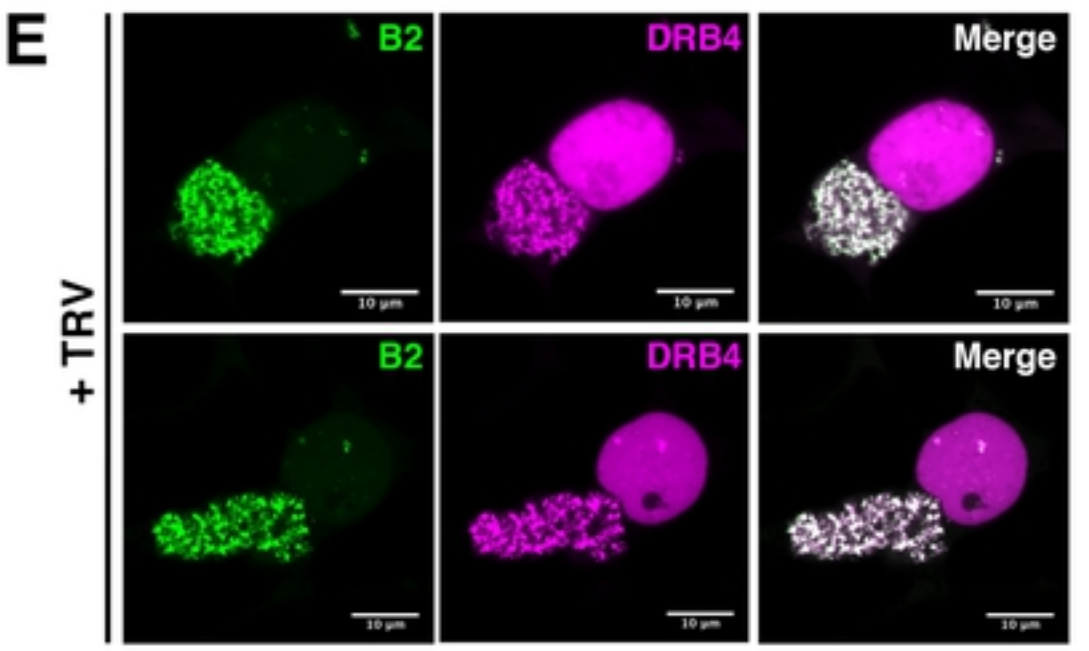
E
+ TRV
B2
DRB4
Merge

Figure 5

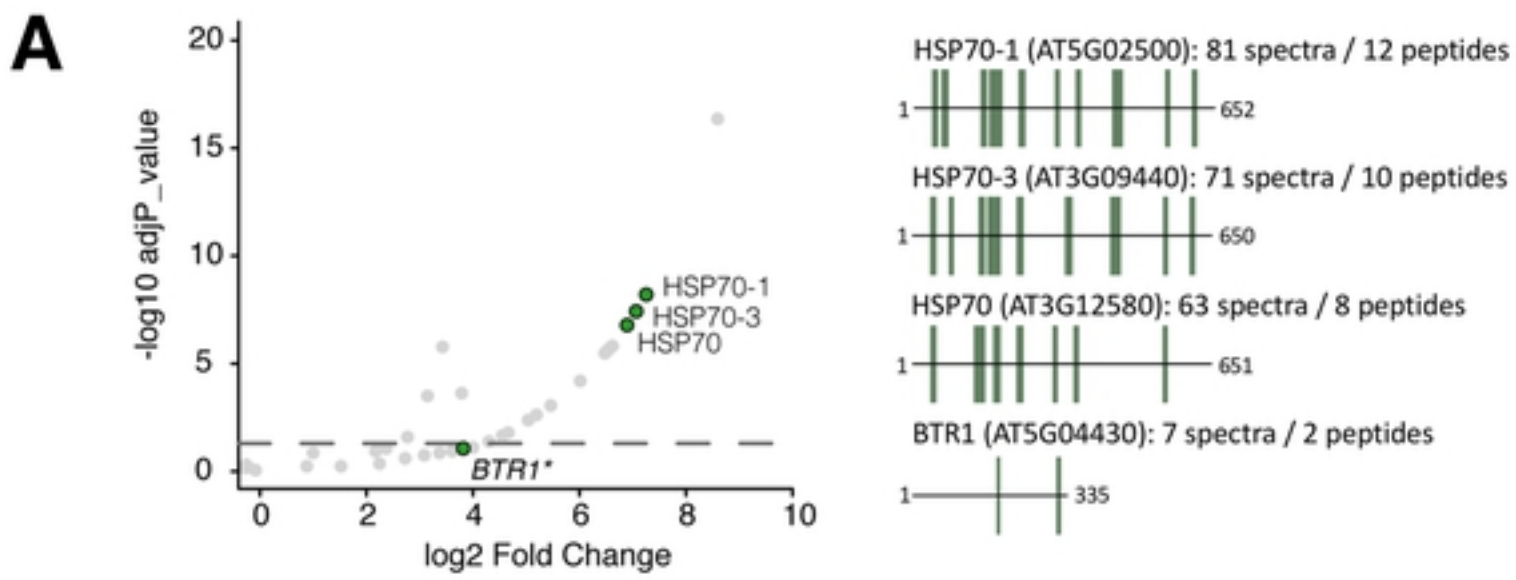
A
-log10 adjP_value
log2 Fold Change
HSP70-1
HSP70-3
HSP70
BTR1*
HSP70-1 (AT5G02500): 81 spectra / 12 peptides
HSP70-3 (AT3G09440): 71 spectra / 10 peptides
HSP70 (AT3G12580): 63 spectra / 8 peptides
BTR1 (AT5G04430): 7 spectra / 2 peptides

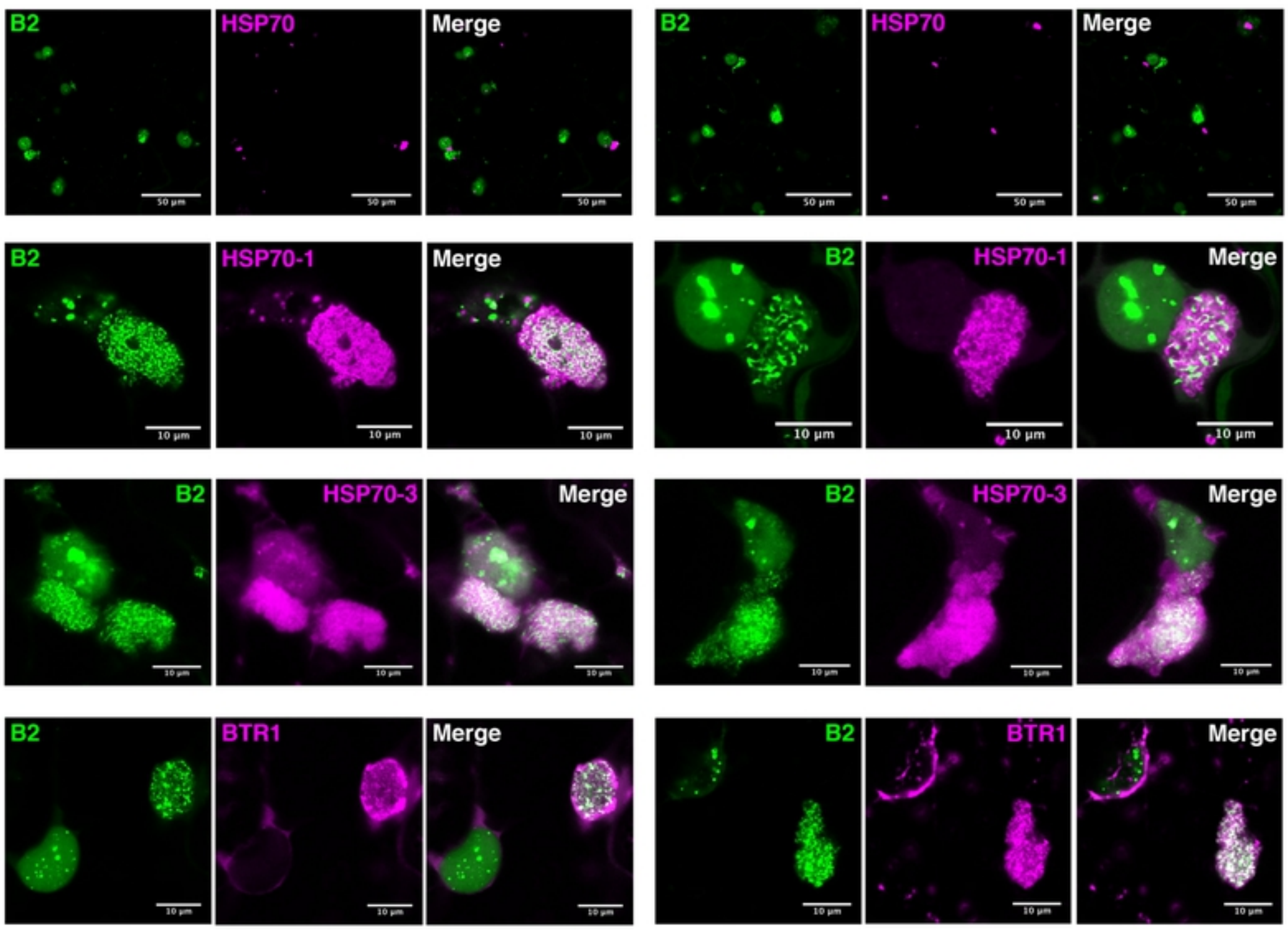
B
B2
HSP70
Merge
C
B2
HSP70-1
Merge
D
B2
HSP70-3
Merge
E
B2
BTR1
Merge

Figure 6

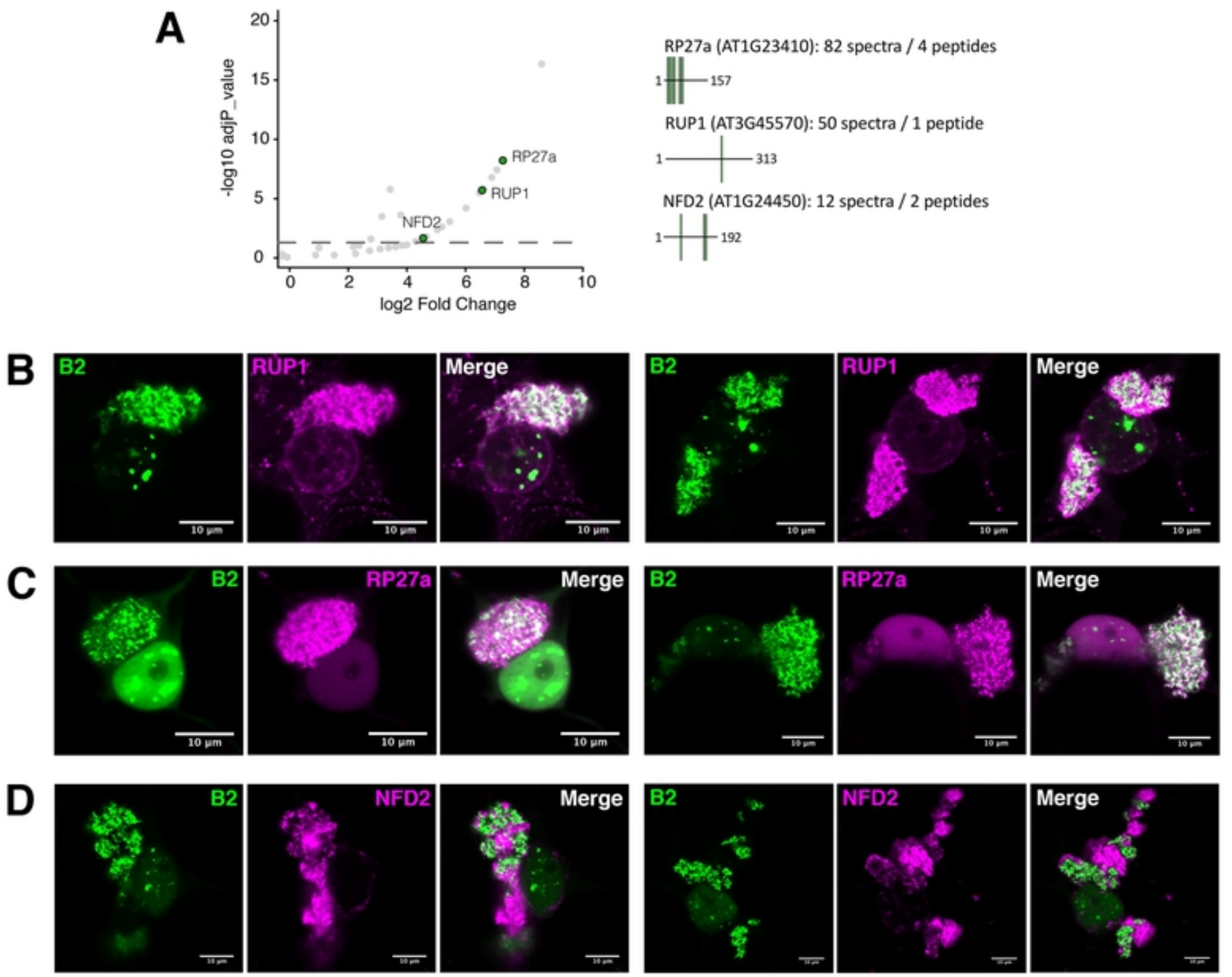
A
-log10 adjP_value
log2 Fold Change
RP27a
RUP1
NFD2
RP27a (AT1G23410): 82 spectra / 4 peptides
RUP1 (AT3G45570): 50 spectra / 1 peptide
NFD2 (AT1G24450): 12 spectra / 2 peptides
B
C
D
B2
RUP1
RP27a
NFD2
Merge
10 µm